Title: Genome-wide *in vivo* CRISPR activation screen identifies BACE1 as a therapeutic vulnerability of lung cancer brain metastasis

Authors: Shawn C. Chafe[1,2]†, Kui Zhai[1,2,3]†, Nikoo Aghaei[4], Petar Miletic[1,2], Zhi Huang[3], Kevin R. Brown[5], Daniel Mobilio[1,2], Daniel Young[6,7], Yujin Suk[1,2], Shan Grewal[1,2], Dillon McKenna[1,2], Zahra Alizada[1,2], Agata M. Kieliszek[1,2], Fred C. Lam[8], Laura Escudero[1,2], Qian Huang[3], Ariana Huebner[9,10], Jack Lu[1,2], Patrick Ang[2,4], Alisha Anand[2,4], Stefan Custers[1,2], Erika Apel[2,4], Sarah Slassi[2,4], Benjamin Brakel[2,4], Jongmyung Kim[11], James K. C. Liu[12], Blessing Iquo Bassey-Archibong[13], Rober Abdo[14,15], Yaron Shargall[1,17], Jian-Qiang Lu[17], Jean-Claude Cutz[17], Qi Zhang[15,18], Shawn Shun-Cheng Li[14], Chitra Venugopal[1,2], Robert E. Hynds[19], Antoine Dufour[6,7], Jason Moffat[5], Charles Swanton[9,10], Shideng Bao[3,19,20]*, Sheila K. Singh[1,2,4]*

Affiliations:
[1]Department of Surgery, McMaster University; Hamilton, ON, Canada.

[2]Centre for Discovery in Cancer Research, McMaster University; Hamilton, ON, Canada.

[3]Department of Cancer Biology, Lerner Research Institute, Cleveland Clinic; Cleveland, OH, USA.

[4]Department of Biochemistry and Biomedical Sciences, McMaster University; Hamilton, ON, Canada.

[5]The Hospital for Sick Children; Toronto, ON, Canada.

[6] Department of Physiology and Pharmacology, Cumming School of Medicine, University of Calgary; Calgary, Alberta, Canada.

[7] Snyder Institute for Chronic Diseases, Hotchkiss Brain Institute and McCaig Institute for Bone and Joint Health, Cumming School of Medicine, University of Calgary; Calgary, AB, Canada.

[8]Department of Neurosurgery, Stanford School of Medicine; Palo Alto, CA, USA.

[9]Cancer Evolution and Genome Instability Laboratory, The Francis Crick Institute; London, England, UK.

[10]Cancer Research UK Lung Cancer Centre of Excellence, UCL Cancer Institute, University College London, Department of Medical Oncology; London, England, UK.

[11]Department of Radiation Oncology, Moffitt Cancer Center; Tampa, FL, USA.

[12]Department of Neuro-oncology, Moffitt Cancer Center; Tampa, FL, USA.

[13]Department of Biological Sciences, Concordia University of Edmonton; Edmonton, AB, Canada.

[14]Department of Biochemistry, Schulich School of Medicine and Dentistry, Western University; London, ON, Canada.

[15]Department of Pathology and Molecular Medicine, Western University; London, ON, Canada.

[16]Division of Thoracic Surgery, McMaster University; Hamilton, ON, Canada.

[17]Department of Pathology and Laboratory Medicine, McMaster University; Hamilton, ON, Canada.

[18]Department of Pathology and Laboratory Medicine, London Health Sciences Centre, London, ON, Canada.

[19]Epithelial Cell Biology in ENT Research Group, Developmental Biology and Cancer Department, UCL Great Ormond Street Institute of Child Health, University College London; London, UK.

[20]Case Comprehensive Cancer Center, Case Western Reserve University School of Medicine; Cleveland, OH, USA.

[21]Center for Cancer Stem Cell Research, Lerner Research Institute, Cleveland Clinic; Cleveland, OH, USA.

*Correspondence: ssingh@mcmaster.ca (S.K.S), baos@ccf.org (S.B)
† - these authors contributed equally

One sentence summary: *in vivo* CRISPR activation screen identifies beta secretase 1 (BACE1) promotes the spread of lung cancers to the brain *via* EGFR signaling.

Abstract:

Brain metastasis occurs in up to 40% of patients with non-small cell lung cancer (NSCLC). Considerable genomic heterogeneity exists between the primary lung tumor and respective brain metastasis; however, the identity of the genes capable of driving brain metastasis is incompletely understood. Here, we carried out an *in vivo* genome-wide CRISPR activation (CRISPRa) screen to identify molecular drivers of brain metastasis from an orthotopic NSCLC patient-derived xenograft model. We discovered activating expression of the Alzheimer's disease associated β-site amyloid precursor protein cleaving enzyme 1 (BACE1) led to a significant increase in brain metastasis. Furthermore, genetic and pharmacological inhibition of BACE1 blocked NSCLC brain metastasis. Mechanistically, we identified BACE1 acts through its novel substrate EGFR to drive this metastatic phenotype. Together, our data highlights the power of *in vivo* CRISPR screening to unveil novel molecular drivers and potential therapeutic targets of NSCLC brain metastasis.

Main Text:

INTRODUCTION

Brain metastasis is a uniformly fatal disease. Arising most commonly from primary tumors originating in the lung, breast and skin, brain metastases (BM) are the most common brain tumor in adults (*1*). It is estimated that approximately 20% of patients with solid tumors will eventually develop BM (*2*). Notably, incidence rates are on the rise, with BM currently matching those of breast and lung cancer (*1*). In the case of lung adenocarcinoma (LUAD), one of the most common sources of BM, 25% of patients will present with, and as many as 50% will eventually develop BM (*3*). Molecular alterations associated with increased likelihood of developing BM from LUAD include activating mutations in *KRAS* and *EGFR*, as well as *ALK* rearrangements (*2*). Survival times for these patients range from 4-15 months, and while molecular targeted therapeutics, including those targeting EGFR and KRAS, have delayed progression-free survival, treatment resistance often develops (*4, 5*). Thus, there is a critical need to improve therapeutic options for patients with BM.

Molecular profiling of BM has identified clonal divergence of the metastatic brain tumor from the primary tumor, revealing both the presence of mutations leading to therapeutic resistance as well as novel actionable mutations not present in the primary tumor (*6*), suggesting particular clones evolve with the capacity to seed BM. Further profiling studies have identified amplification of *MYC*, *YAP1* and *MMP13* are associated with increased development of LUAD-BM (*7*). While critical to our understanding of clonal evolution of BM, these analyses overlook the importance of non-mutated genes in the development of BM. To this end, *TWIST2* and *SPOCK1* have been shown to be important for

supporting growth of non-small cell lung cancer (NSCLC) BM through loss-of-function screening in brain metastasis initiating cells (BMICs) (*8*). While analyses of transcriptional signatures associated with LUAD-BM have identified the importance of WNT/TCF (*9*), STAT3 (*10*), serpins (*11*) and HLA-G (*12*), these studies do not address whether expression of these genes is sufficient for driving dissemination from the lung to the brain. Here, we employed a genome-wide *in vivo* CRISPR activation screen to identify drivers of NSCLC BM from orthotopic LUAD tumors. In doing so, we identified the β-site amyloid precursor protein cleaving enzyme 1, also known as β-secretase 1, (*BACE1*) as an important regulator of NSCLC dissemination to and colonization of the brain. Mechanistically, we found that BACE1 acts through EGFR to promote metastatic phenotypes.

RESULTS

In vivo CRISPR activation screen identifies BACE1 as a driver of lung adenocarcinoma brain metastasis

To identify genetic drivers promoting the spread of LUAD to the brain in a clinically-relevant model, we made use of a primary LUAD patient-derived cell line CRUK0748-XCL, which originates from a patient-derived xenograft derived within the TRACERx study (Table S1) (*13*). We modified the cell line to express the catalytically inactive dCas9 (*14*) fused to VP64 (*15*) (fig. S1A), GFP and luciferase in order to activate gene transcription and to permit tracking of these cells *in vivo*, respectively and known from here onwards as CRUK0748-XCL-GLD cells. We confirmed the ability of dCas9 expression to induce target gene expression in cells *in vitro* by inducing CD45 expression following

transduction of the CRUK0748-XCL-GLD cells with sgRNA to *PTPRC* (fig. S1B). We then proceeded to screen for genes whose expression would enhance BM from an orthotopic LUAD tumor. To do this, we utilized the human Calabrese genome-wide CRISPRa library (*16*). CRUK0748-XCL-GLD cells were transduced with the library at an MOI of 0.3 and selected to yield a final library coverage of 500x (Fig. 1A). We inoculated library-transduced cells directly into the lungs of 30 NSG mice using a modified thoracotomy procedure, providing 35x coverage of the library per mouse, as we have described previously in our established brain metastasis models (*8, 10, 12, 17*). We then followed tumor burden longitudinally by bioluminescent imaging. At endpoint, lungs and brains were collected and brains imaged by bioluminescent imaging to confirm the presence of metastases (fig. S1C). Genomic DNA extracted from both lungs and brains was sequenced to determine single guide RNA (sgRNA) abundance and identity. We started with sgRNAs targeting 18,885 genes present in our cell inoculum which was confirmed by sequencing of the T_0 pellet (Fig. 1B). At endpoint we detected similar sgRNA representation in the lungs across all mice sequenced, suggesting that variability in engraftment rates would not impact our discovery approach (fig. S1D). Looking at the distribution of the sgRNA sequences in the lungs and the brains revealed an enrichment of a subset of gene targeting sgRNAs (fig. S1, E and F). Indeed, when we sequenced sgRNA sequences from the brains, we detected the presence of at least 1 sgRNA targeting 6862 unique genes. We then filtered our gene list by prioritizing genes with greater than one sgRNA present in the brains across all mice with an average abundance for the sgRNA in the brain cohort greater than in the lungs. Moreover, we also included genes with a single sgRNA enriched in the brain if the gene had 2 or fewer targeting

sgRNAs detected in the lungs, which narrowed our list to 28 genes (Fig. 1B). Notably, since we expressed sgRNA as an enrichment in the brains relative to the lung this allowed us to select against genes involved in regulating proliferation where any enhancement in proliferation would be evident in both compartments. Indeed, none of the genes identified in our top 28 were known regulators of cell proliferation. Interrogating The Cancer Genome Atlas (TCGA) and DepMap (*18*) databases to prioritize genes broadly expressed in cancer and whose loss negatively affected cell viability across a panel of cancer cell lines, our list was further distilled to 12 genes which had an increased relative abundance of sgRNAs targeting them in the brain over the lung (Fig. 1, C and D, and Table S2). Among the genes in our shortlist was *CTSF*, the gene encoding cathepsin F. Cathepsin F was recently implicated as a biomarker of LUAD BM (*19*), adding independent biological validation to one of our hits and confirming the screen strategy was capable of identifying biologically relevant drivers of BM. Furthermore, cathepsin S, another member of the cathepsin family, has previously been shown to promote BM (*20*). We also implicated genes involved in lipid metabolism (*PLIN5*, *FADS1*, *D2HGDH*) which has been shown to be important for BM (*21, 22*). Moreover, genes previously identified in our BMIC gene signature as well as associated with brain tumor initiating cells (*IMPDH2*, *PROM1*) were also detected, independently confirming our previous findings and further supporting the validity of our strategy (*23-25*). In addition, we identified genes (*KLHL12*, *SENP8*) involved in regulating post-translational modifications of proteins, specifically CUL3, through ubiquitylation and NEDDylation, respectively, reinforcing the role of CUL3 in NSCLC (*26, 27*). Lastly, we identified sgRNA targeting *BACE1* were enriched greater than 150-fold in the brains of the mice in our cohort (Fig. 1D). Importantly, *BACE1*

expression was elevated in our BMIC signature derived from disseminated lung cancer cells in the brain (*12*). Furthermore, we recently identified BACE1 was important for maintaining a tumor-promoting macrophage phenotype in glioblastoma, suggesting it might have a multi-faceted role in the progression of solid cancers in the brain (*28*). BACE1 is primarily known for its role in Alzheimer's disease (AD) (*29*). It is a single-pass transmembrane protein member of the aspartyl protease family that is required for the production of amyloid-β (Aβ) peptide, which accumulates in the brains of patients with AD (*29*). Since *BACE1* has never been previously implicated in LUAD or BM, we decided to investigate its role in greater depth.

To confirm elevated *BACE1* expression in primary LUAD increased BM, we generated CRUK0748-XCL-GLD cells expressing the top two most efficacious *BACE1*-targeting sgRNAs from the screen (fig. S1G). We inoculated these cells directly into the lungs of NSG mice and followed tumor burden over time by bioluminescent imaging (Fig. 1E). As mouse endpoint in this model is dictated by primary lung tumor burden, we extracted brains at endpoint and imaged them by *ex vivo* bioluminescence imaging to detect metastatic brain signal (Fig. 1F). Consistent with the high ranking of *BACE1* in the screen, and in support of our primary screen findings, activation of its expression with two independent sgRNAs increased metastatic brain tumor burden (Fig. 1, F and G). Furthermore, we interrogated liver and bone for the presence of metastases to determine whether BACE1 expression could also enhance the spread of LUAD cells to these distant sites. Indeed, we observed increased metastatic burden in the livers as well as in the bones of mice with BACE1 over-expressing lung tumours (fig. S1, H and I). Together, these data provide additional validation for our pooled CRISPRa screen finding that

increased expression of *BACE1* enhances LUAD BM while also providing evidence that BACE1 expression may predict LUAD metastasis.

BACE1 **is expressed in LUAD brain metastases and is associated with shorter survival**

To evaluate whether BACE1 expression is clinically relevant in NSCLC, we stained a NSCLC tumor microarray (TMA) consisting of primary LUAD (Fig. 2A) and lung squamous cell carcinomas (LUSC; fig. S2, A and B) for BACE1. We found that BACE1 was highly expressed in 71% of all cores present in the TMA, suggesting BACE1 might be a biologically relevant molecule in NSCLC. Furthermore, we looked into the TRACERx 421 cohort for associations of *BACE1* expression with clonal driver mutations linked to the development of BM (fig. S2C). We found that *BACE1* expression was highest in *EGFR* mutant LUAD. We next assessed whether expression of BACE1 was also present in BM from patients with LUAD. We found that BACE1 was expressed in all 13 metastatic brain tumors interrogated (Fig. 2B, fig. S2D, and Table S3), but not in adjacent normal areas or most normal tissues outside of the brain (fig. S2, E and F). Additionally, we possessed two matched primary LUAD-BM pairs in our biobank that we were able to interrogate and assess whether BACE1 expression was preserved from primary to metastatic brain tumor (Fig. 2C, and Table S3). Notably, BACE1 expression in the primary tumor was maintained in the BM. Moreover, when we evaluated BACE1 expression in NSCLC tumors from patients that did not develop BM, BACE1 staining was minimal (fig. S2G). We then looked to extend these observations to an additional cohort of BM patients and stained a TMA consisting of 44 matched primary NSCLC and their matched BM for BACE1 (Fig. 2D)

(*30*). BACE1 staining was detected in all but 3 primary lung tumours, yet was detected in the BM of all patients (Fig. 2E). Interestingly, the expression of *BACE1* at the RNA level in these cores was quite stable between the primary and BM, suggesting that BACE1 expression may be regulated post-translationally in LUAD (Fig. 2F). We then assessed whether *BACE1* expression in BM was associated with patient survival. Stratifying patients according to BACE1 expression in the London Health Sciences cohort revealed that those patients with high BACE1 expression in their BM survived for much shorter times from their BM diagnosis than those with lower BACE1 expression (Fig. 2G). We next interrogated the LUAD TCGA data where the metastatic status was available and found information for 34 patients with BM. When we stratified this patient cohort according to median expression of *BACE1*, those with high *BACE1* expression survived for a shorter duration than those with low *BACE1* expression (Fig. 2H). Moreover, we ran a multivariate analysis cox proportional hazards model with age, sex, stage and smoking status as co-variates and determined that high BACE1 expression was indeed associated with worse outcomes in both cohorts (HR^{LHSC} = 2.64, p=0.008; HR^{TCGA} = 1.98, p=0.004). Together, these data suggest that BACE1 is a clinically relevant target in NSCLC, expressed in both primary lung tumors and NSCLC brain metastases (LBM) where its expression is associated with worse prognosis.

BACE1 drives migration and invasion of primary LUAD

To evaluate the biological relevance of BACE1 expression in LUAD and LBM, we assessed BACE1 expression in a panel of LUAD and patient-derived LBM cell lines in our biobank to adopt suitable models for further investigation (Fig. 3A and fig. S3A). To

163 determine whether BACE1 expression supported aggressive phenotypes, we first
164 evaluated whether BACE1-expressing cells were more migratory. Indeed, activation of
165 BACE1 enhanced migration of CRUK0748-XCL-GLD cells through transwell membranes
166 (Fig. 3B, and fig. S3B). In order to assess whether BACE1 expression was necessary for
167 LUAD migration, we genetically deleted *BACE1* using CRISPR/Cas9 in CRUK0748-XCL
168 cells (fig. S3C). In contrast to increased expression of BACE1, suppressing BACE1
169 expression reduced the migratory capacity of these cells (Fig. 3C, and fig. S3D). We next
170 investigated whether BACE1 activity was required for the increased migration associated
171 with BACE1 expression. To address this question, we made use of Verubecestat (MK-
172 8931), a potent, blood-brain barrier permeable, small molecule inhibitor targeting BACE1
173 that has been trialed in AD (*29, 31*). Indeed, the increased migration associated with
174 higher BACE1 expression was dependent upon BACE1 activity as MK-8931 reduced the
175 ability of CRUK0748-XCL cells to migrate (Fig. 3D, and fig. S3E).
176 We next evaluated whether BACE1 expressing cells were more invasive using a spheroid
177 invasion assay. We knocked BACE1 expression out in H1299 NSCLC cells and
178 assessed their capacity to invade through Matrigel™ (fig. S3F). Suppression of BACE1
179 expression attenuated the invasive capacity of these cells (Fig. 3, E and F). Conversely,
180 over-expression of BACE1 enhanced their invasive capacity (Fig. 3G, and fig. S3G).
181 Moreover, this invasive phenotype was dependent upon BACE1 activity, as MK-8931
182 impeded their ability to invade (Fig. 3H). However, to truly assess the role of BACE1 in
183 invasion, we made use of a non-metastatic patient-derived primary LUAD line,
184 CRUK0733-XCL, and assessed whether increased BACE1 expression was sufficient to
185 drive invasion (fig. S3H). Increased BACE1 expression in CRUK0733-XCL led to an

increase in the invasive capacity of these cells (Fig. 3, I and J, Movies S1 and S2). Together these data support a cell-autonomous role for BACE1 in enhancing the invasive phenotype of NSCLC cells.

BACE1 is required for the proliferation and self-renewal capacity of LUAD brain metastasis initiating cells

Since BACE1 supported phenotypes associated with LUAD dissemination, we next wanted to assess the role of BACE1 in brain metastatic LUAD cells. To assess whether BACE1 expression was important for LBM growth, we disrupted *BACE1* using CRISPR/Cas9 in the patient-derived MH1002 and MH1012 LBM lines (Fig. 4A, and Table S1) and assessed cell proliferation (Fig. 4B). Loss of BACE1 expression reduced LBM cell proliferation in both cell lines (Fig. 4B). We next grew MH1002 and MH1012 in stem cell enriching conditions to assess whether BACE1 was important for LBM self-renewal, a cardinal stem cell property (Fig. 4C). Similar to what we observed in our NSCLC models, loss of BACE1 expression reduced sphere forming capacity and sphere size in both LBM lines (Fig. 4, C and D, fig. S4A). Together, these findings suggest that BACE1 expression is important for LBM growth and self-renewal capacity.

BACE1 enzymatic activity is important for the growth and self-renewal of LUAD LBM cells

We next assessed whether BACE1 enzymatic activity was also important for LBM proliferation and self-renewal capacity. We therefore tested the effect of MK-8931 on the growth of our patient-derived LBM cells. MK-8931 treatment of MH1002, MH1012, BT530 and BT478 reduced cell proliferation in a target-specific and dose-dependent manner

(Fig. 4E, and fig. S4B and C). Moreover, we confirmed these findings with three additional BACE1 inhibitors, AZD3293, AZD3839, and PF-06751979 in MH1002 cells (fig. S4D). We next investigated whether BACE1 activity supported the self-renewal capacity of MH1002 and MH1012 cells (Fig. 4F). Growth of MH1002 and MH1012 in stem cell enriching conditions in the presence of MK-8931 reduced their ability to form spheres (Fig. 4G). Moreover, we made similar observations in CRUK0748-XCL and H1299 NSCLC cells (fig. S4, E to H). Collectively, these data confirm our genetic findings and suggest that BACE1 activity is important for sustaining the growth and self-renewal of LBMs, properties critical for supporting initiation and maintaining growth of disseminated cells in the brain.

BACE1 is required for LUAD brain metastasis

After demonstrating that genetically and pharmacologically perturbing BACE1 expression and activity, respectively, altered the growth and invasiveness of NSCLC and LBM lines *in vitro*, we wanted to assess whether we could limit the spread of BACE1-expressing disseminated LUAD cells to the brain by targeting BACE1 activity with MK-8931. To do this, we made use of our CRUK0748-XCL primary LUAD model expressing *BACE1*-activating sgRNA, and implanted these cells directly into the lungs of NSG mice (Fig. 5A). We allowed tumors to form for seven days before randomly assigning *BACE1*-activated, or control, tumor bearing mice to vehicle or MK-8931 treatment groups. Mice were treated daily for three weeks and then all mice were culled to assess any differential in metastatic brain tumor burden (Fig. 5B). Bioluminescence imaging of brains collected at endpoint confirmed increased expression of BACE1 enhanced the metastatic propensity of

CRUK0748-XCL-GLD cells (Fig. 5, B and C). Moreover, MK-8931 treatment reduced the spread of this primary LUAD model to the brain (Fig. 5, B and C). Notably, MK-8931 had minimal impact on the wild-type cells which are much more inefficient at reaching the brain and express lower amounts of BACE1 (fig. S1G). Together, these data support a critical role for BACE1 activity in all stages of the development of LUAD BM.

BACE1 expression is required for growth of established LBM

BM patients often present clinically with symptomatic lesions. To test whether we could target BACE1 in a setting of advanced disease, we used our orthotopic, intracranial implantation BM model. Given the link between self-renewal capacity *in vitro* and tumor initiating capacity *in vivo* (*32*), we first assessed whether BACE1 expression was important for LBM tumor growth in the brain. To test this, we inoculated MH1002 *BACE1*^{KO} or control (*AAVS1*^{KO}) cells into the brains of immunocompromised mice and monitored tumor growth (Fig. 5D). We found that loss of BACE1 expression markedly impaired LBM tumor growth in the brain, which resulted in a considerable extension in survival (Fig. 5, E and F). Since BACE1 expression was required for sustaining LBM growth in the brain, we next assessed whether MK-8931 would also impact the growth of LBM in the brain. MH1002 cells were inoculated into the brain of NSG mice, allowed to form tumors for seven days, after which time MK-8931 was administered daily for three weeks (Fig. 5G). Treatment with MK-8931 reduced LBM brain tumor growth, which led to a marked extension in survival (Fig. 5, H to J). Collectively, these data confirm that BACE1 plays an essential role in LBM cell and tumor growth and provide evidence that

254 targeting BACE1 with the BBB permeable MK-8931 represents a clinically relevant
255 approach to treat BM.

256 **BACE1 activates the EGFR/MEK/ERK signaling pathway in NSCLC cells**

257 BACE1 is the rate-limiting enzyme in the production of Aβ. While critical for the
258 pathogenesis of AD, Aβ has also recently been implicated in playing an instrumental role
259 in the development of melanoma BM(*33*). To address whether Aβ was involved in our
260 lung cancer system, we measured Aβ secretion into the conditioned media of WT or
261 BACE1-activated CRUK0748-XCL cells (fig. S5A). Interestingly, Aβ concentrations were
262 nearly undetectable in the conditioned media from CRUK0748 cells and decreased when
263 we increased BACE1 expression, suggesting that Aβ is not instrumental in supporting
264 BACE1-dependent LUAD BM in our model (fig. S5A). To uncover the underlying
265 molecular mechanisms by which BACE1 promotes the metastatic potential of LBM cells,
266 we performed a phospho-kinase array screen to identify potential kinases whose activity
267 might be modulated by BACE1. Loss of BACE1 expression resulted in decreased
268 phosphorylation of EGFR, ERK1/2, and cJun (Fig. 6A and fig. S5B). Decreased
269 phosphorylation of EGFR, ERK1/2 and cJun would be consistent with decreased
270 proliferation, self-renewal and migration capacity supporting our earlier findings in the
271 absence of BACE1 (*34*). We next confirmed the findings of the antibody array by
272 interrogating the associated signaling cascades directly (Fig. 6B). Similar to the antibody
273 array, abrogation of BACE1 expression by CRISPR/Cas9 with two independent sgRNAs
274 resulted in decreased phosphorylation of EGFR, MEK1/2, ERK1/2 and cJun in MH1002
275 and H1299 cells (Fig. 6B, fig. S5, C and D, and Table S1), indicating the entire MEK/ERK
276 pathway downstream of EGFR was affected by BACE1 expression. Furthermore, we

also observed consistent decreases in activation of EGFR, MEK1/2, ERK1/2 and cJun following treatment with MK-8931 in both MH1002 and H1299 cells (Fig. 6C, and fig. S5, E and F). We next interrogated MH1002 tumors that had been treated with MK-8931 for activation of EGFR. While vehicle treated tumors contained considerable EGFR activation marked by tyrosine 1068 phosphorylation, MK-8931 treated tumors contained greatly reduced EGFR activation (Fig. 6, D and E). Together, these data confirm that BACE1 activity is important for maintenance of EGFR/MEK/ERK signaling.

We next sought to confirm this axis was responsible for the brain metastatic phenotype promoted by BACE1 expression. To do this we expressed a constitutively active EGFR ($EGFR^{L858R}$) in $BACE1^{KO}$ $H1299^{GFP\text{-}Luc}$ primary LUAD cells (Fig. 6F). The presence of $EGFR^{L858R}$ is one of the most prevalent activating point mutations in EGFR present in patients with EGFR mutant LUAD (*35*). After confirmation of transgene expression, we evaluated whether constitutive activation of EGFR downstream of BACE1 loss would impact the ability of the cells to invade (Fig. 6G). Indeed, expression of $EGFR^{L858R}$ was able to restore the invasive capacity of $H1299^{GFP\text{-}Luc}$ $BACE1^{KO}$ cells (Fig. 6, G and H). We next assessed whether this restored invasive capacity would translate to restoration of a BM phenotype *in vivo*. To do this, we implanted $H1299^{GFP\text{-}Luc}$ $BACE1^{KO}$ or $BACE1^{KO}$:$EGFR^{L858R}$ cells directly into the left ventricle of NSG mice (Fig. 6I). At endpoint, bioluminescent imaging of the brains confirmed that $BACE1^{KO}$ cells were unable to efficiently seed BM (Fig. 6, J and K). However, reconstitution of active EGFR in $BACE1^{KO}$ cells ($BACE1^{KO}$:$EGFR^{L858R}$) was able to restore the brain metastatic phenotype of BACE1-deficient cells, demonstrating that restoring EGFR signalling can compensate

for the defects in brain metastatic capacity associated with BACE1 loss and the concomitant blunting of the pathway downstream of EGFR. (Fig. 6, J and K).

EGFR is a novel substrate of BACE1

Since BACE1 activity in our models has been important for promoting the spread of LUAD to the brain and for influencing cellular biochemical signaling starting from EGFR at the plasma membrane, we next investigated whether the protease activity of BACE1 might have a role in cleaving EGFR. To test this hypothesis, we investigated whether BACE1 and EGFR interacted *in situ* to support a mechanism whereby BACE1 cleaves EGFR directly. We looked into this more closely in HEK293T cells, where neither BACE1 nor EGFR are highly expressed under endogenous conditions (Fig. 7A). We transfected cells with plasmids expressing full length BACE1 and/or EGFR which led to robust expression of both proteins (Fig. 7A). We then performed proximity ligation assays (PLA) to assess whether the two proteins were close enough to physically interact in cells (*36*). Robust PLA signal was detected in cells expressing both EGFR and BACE1, but not in cells expressing each gene individually (Fig. 7, B and C). To rule out that this was due to over-expression of both BACE1 and EGFR, we performed PLA assays in MH1002 cells that endogenously express BACE1 and EGFR (Fig. 7D). Here again, robust PLA signal was observed, suggesting that BACE1 is in close enough proximity to interact with and mediate direct cleavage of EGFR in cells (Fig. 7, D and E).

To address the possibility that BACE1 could cleave EGFR directly, we co-incubated the recombinant catalytic domain of BACE1 (rBACE1) with the recombinant ectodomain of EGFR (rEGFR) while varying their molar ratios (Fig. 7F). Increasing amounts of rBACE1

led to increasing cleavage of rEGFR when incubated in buffer where BACE1 activity is maximal (pH 4.0). In contrast, when we combined the two proteins together in buffer where rBACE1 is inactive (pH 7.0), with the same molar ratios, we did not detect any cleavage of rEGFR supporting our observations that the cleavage of rEGFR was dependent upon BACE1 activity. To identify the cleavage sites of BACE1 within EGFR we utilized a highly sensitive mass spectrometry technique that would allow for the detection of neo-N-termini (protease cleavage sites) known as amino-terminal oriented mass spectrometry of substrates (ATOMS) (*37*). A mixture of rEGFR was dimethylated with light formaldehyde (CH_2O, +28 Da) and a mixture of rEGFR co-incubated with rBACE1 was dimethylated with deuterated/heavy formaldehyde (CD_2O; +34 Da). Both mixtures were combined and then subjected to LC-MS/MS followed by MaxQuant analysis (Fig. 7G). After a 24 hour co-incubation of rBACE1 and rEGFR, 9 cleavage sites were identified: $^{4}S\downarrow G^{5}$, $^{53}R\downarrow M^{54}$, $^{119}L\downarrow A^{120}$, $^{130}T\downarrow G^{131}$, $^{146}G\downarrow A^{147}$, $^{305}G\downarrow S^{306}$, $^{410}W\downarrow P^{411}$, $^{475}I\downarrow N^{476}$, $^{502}T\downarrow G^{503}$ distributed throughout domains I-IV (Fig. 7H and Table S5). Since a prominent band was detected around ~10 kDa following co-incubation of rBACE1 and rEGFR, we focused on cleavage sites $^{119}L\downarrow A^{120}$, $^{130}T\downarrow G^{131}$, $^{146}G\downarrow A^{147}$. To validate the cleavage site directly, we measured BACE1 activity towards a peptide encompassing these cleavage sites labelled with FRET donor:acceptor pairs methyl coumarin and dinitrophenol (Fig. 7I and fig. S6A). Co-incubation of rBACE1 with the fluorogenic peptide containing the $^{119}L\downarrow A^{120}$ cleavage site, but not the peptide alone, produced fluorescent signal, which was dependent upon BACE1 activity as MK-8931 treatment blocked the production of a detectable fluorescent signal (Fig. 7I). Moreover, no BACE1 activity could be detected towards $^{130}T\downarrow G^{131}$, $^{146}G\downarrow A^{147}$ sites during the reaction suggesting the

345 ^{119}L↓A^{120} cleavage site was the predominant cleavage site in that region of the protein
346 (fig. S6A). Together, these data confirm EGFR to be a novel substrate of BACE1.
347 Next, we addressed whether BACE1 could cleave EGFR in cells. To do this, we once
348 again transiently expressed BACE1 and EGFR in HEK293T cells (Fig. 7J). Probing for
349 EGFR with an antibody specific to an N-terminal epitope consisting of amino acids 129-
350 160 revealed EGFR expression in cell lysates decreased as BACE1 expression
351 increased. Next, we probed conditioned medium from cells in which these lysates were
352 collected for the N-terminal fragment of EGFR (129-160) and observed a concomitant
353 increase in the presence of this N-terminal peptide in response to increasing amounts of
354 BACE1 expression in these cells (Fig. 7J), strongly suggesting that BACE1 was mediating
355 the cleavage of EGFR in cells. Based on our findings, BACE1 inhibition would not be
356 predicted to have much effect on the growth of EGFR mutant LUAD lines. To test this
357 directly, we treated EGFR mutant LUAD lines PC9 and H1975 with MK-8931 (fig. S6, B
358 to D). Indeed, MK-8931 treatment did not have much of an effect of the growth of these
359 lines. Furthermore, since Osimertinib is administered in a front-line setting to patients
360 with EGFR mutant LUAD (*5*), we tested whether there was any potential interaction
361 between the two drugs in these models (fig. S6, E and F). In agreement with our MK-
362 8931 studies, and data up to this point, there was a lack of any synergy between the two
363 drugs. However, importantly there was also absence of any antagonistic effects of the
364 two drugs suggesting that they may be co-administered without any impact on the efficacy
365 of EGFR inhibition.
366 In summary, our findings support a model whereby BACE1 promotes LUAD brain
367 metastasis *via* its novel substrate EGFR.

DISCUSSION

There are very few effective treatment options available for patients with BM. In this study, we developed an *in vivo* CRISPRa screen in an orthotopic patient-derived LUAD model to identify putative drivers of BM which could potentially serve as future biomarkers and/or therapeutic targets for this deadly disease. We identified BACE1 as a critical enzyme involved in enhancing the invasive, proliferative and initiation capacity of primary and brain metastatic LUAD cells by activating the EGFR/MEK/ERK cellular signaling axis. Our study thus identifies a new therapeutic target to be explored for BM.

Verubecestat (MK-8931) is the first BACE1 inhibitor to advance to phase 3 clinical trial (*38*) and is generally safe and well-tolerated in healthy adults (*39*) and AD patients (*29, 31*). Although targeting BACE1 by Verubecestat is not effective for treating AD patients (*29*), our studies and the fact that this drug is blood-brain barrier penetrant, strongly indicate that it can be repurposed for treatment of BM, highlighting the potential of BACE1 as a novel target for treating lung cancer. In support of our findings, Aβ secretion from melanoma cells was recently shown to facilitate the growth of melanoma cells in the brain which could be reduced through the use of a BACE inhibitor (*33*). While our study does not support a role of amyloid precursor protein (APP) or Aβ in BACE1-mediated BM in our models, the importance of BACE1 in modulating EGFR signaling is clear, and future work to evaluate the utility of Aβ as a biomarker for lung cancer BM as a surrogate for BACE1 expression/activity is warranted.

391 EGFR plays a fundamental role in cancer biology and especially NSCLC biology (*40*).
392 Here we identify EGFR is a novel substrate of BACE1. Cleavage of EGFR between L^{119}
393 and A^{120} is predicted to disrupt the four interactions EGF makes with the receptor in
394 domain I at L^{14}, Y^{45}, L^{69} and L^{98} (*41*). While this cleavage might induce conformational
395 changes to influence ligand binding, receptor dimerization and activation, future studies
396 are needed to fully appreciate the biophysical and biochemical changes to EGFR
397 following cleavage by BACE1. The implications of this finding are far reaching, as
398 therapeutic targeting of EGFR in NSCLC has revolutionized patient care, greatly
399 extending survival times over chemotherapy, although drug resistance remains a
400 challenge (*5*). Here, we demonstrate that in instances where EGFR is wild-type, which
401 accounts for more than half of all patients with LUAD (*40*), BACE1 is needed for activation
402 of EGFR and downstream signaling. This suggests that a patient population otherwise
403 not being considered for EGFR-targeting tyrosine kinase inhibitors in a front-line setting
404 due to lack of mutations detected by sequencing, may benefit from such a therapy if
405 BACE1 is present in their tumor. Based on our findings, therapeutic targeting of BACE1
406 may not be predicted to benefit patients with activating mutations in EGFR; however, our
407 data in EGFR mutant LUAD models indicates MK-8931 and osimertinib are not
408 antagonistic suggesting that the two may be co-administered without any deleterious
409 effects of one drug on the other's efficacy. Nevertheless, our data are supportive of
410 targeting BACE1 in KRAS driven lung cancers which also have a strong predilection to
411 end up in the brain (*42*). Evidence exists in other cancers demonstrating EGFR activity
412 is needed for full activation of MEK and ERK downstream of mutant KRAS and this may

be the first example of that in NSCLC (*43*), reinforcing a need to target BACE1 in this setting.

A limitation to our study is that our models are patient-derived and engrafted in immunocompromised mice omitting the contribution of the immune system to the development of BM. However, since our screen was conducted with these models and identified the cell autonomous role of BACE1 in the development of lung cancer brain metastasis, these findings are likely to be conserved in the presence of immune cell populations. Nevertheless, addressing the contribution of the immune system to our findings will be the subject of future investigations.

In conclusion, our *in vivo* CRISPR activation screen identified BACE1 as a novel, tractable target for LUAD BM. In light of these findings, we suggest repurposing drugs designed to target BACE1 for AD, in particular Verubecestat, in LUAD to suppress the development of BM.

MATERIALS AND METHODS

Study design

This study was designed to identify genes promoting the spread of NSCLC to the brain. Preclinical patient-derived animal models of NSCLC and BM that arose from NSCLC were utilized to investigate the role of BACE1 in BM and for therapeutic intervention studies. Sample sizes were chosen based on effect sizes based on pilot experiments and no statistical method was used to predetermine sample size. The indicated sample size

represents biological replicates and each experiment was performed two to three times. Replicates were only excluded if indicated to be true outliers by the Grubb's test. For *in vivo* studies mice were randomly assigned to treatment group. Investigators were not blinded to treatment group during data collection and analysis.

Statistics

All bar graphs plot the mean ± SEM or mean ± SD as indicated. Significant differences were determined between two groups using the two-way Student's t-test and Mann-Whitney U test for non-parametric data or among multiple groups using one-way ANOVA with Sidak's or Tukey's multiple comparisons tests *post-hoc* or two-way ANOVA and statistical significance was set at $p < 0.05$. Survival analysis was performed using the Log-rank test. All analyses were performed with GraphPad Prism 9 software (https://www.graphpad.com/). Multivariate analyses were run using a cox proportional hazards model in R using age, sex, stage and smoking status as covariates (*51*). Experimental details such as number of animals or cells and experimental replication were provided in the figure legends. Data inclusion/exclusion criteria was not applied in this study.

List of Supplementary Materials

Figs. S1 to S6
Tables S1 to S6
Movies S1 and S2

References and Notes

1. A. A. Aizer, N. Lamba, M. S. Ahluwalia, K. Aldape, A. Boire, P. K. Brastianos, P. D. Brown, D. R. Camidge, V. L. Chiang, M. A. Davies, L. S. Hu, R. Y. Huang, T. Kaufmann, P. Kumthekar, K. Lam, E. Q. Lee, N. U. Lin, M. Mehta, M. Parsons, D. A. Reardon, J. Sheehan, R. Soffietti, H. Tawbi, M. Weller, P. Y. Wen, Brain metastases: A Society for Neuro-Oncology (SNO) consensus review on current management and future directions. *Neuro Oncol* **24**, 1613-1646 (2022).

2. A. S. Achrol, R. C. Rennert, C. Anders, R. Soffietti, M. S. Ahluwalia, L. Nayak, S. Peters, N. D. Arvold, G. R. Harsh, P. S. Steeg, S. D. Chang, Brain metastases. *Nat Rev Dis Primers* **5**, 5 (2019).
3. D. N. Cagney, A. M. Martin, P. J. Catalano, A. J. Redig, N. U. Lin, E. Q. Lee, P. Y. Wen, I. F. Dunn, W. L. Bi, S. E. Weiss, D. A. Haas-Kogan, B. M. Alexander, A. A. Aizer, Incidence and prognosis of patients with brain metastases at diagnosis of systemic malignancy: a population-based study. *Neuro Oncol* **19**, 1511-1521 (2017).
4. P. A. Janne, G. J. Riely, S. M. Gadgeel, R. S. Heist, S. I. Ou, J. M. Pacheco, M. L. Johnson, J. K. Sabari, K. Leventakos, E. Yau, L. Bazhenova, M. V. Negrao, N. A. Pennell, J. Zhang, K. Anderes, H. Der-Torossian, T. Kheoh, K. Velastegui, X. Yan, J. G. Christensen, R. C. Chao, A. I. Spira, Adagrasib in Non-Small-Cell Lung Cancer Harboring a KRAS(G12C) Mutation. *N Engl J Med* **387**, 120-131 (2022).
5. J. C. Soria, Y. Ohe, J. Vansteenkiste, T. Reungwetwattana, B. Chewaskulyong, K. H. Lee, A. Dechaphunkul, F. Imamura, N. Nogami, T. Kurata, I. Okamoto, C. Zhou, B. C. Cho, Y. Cheng, E. K. Cho, P. J. Voon, D. Planchard, W. C. Su, J. E. Gray, S. M. Lee, R. Hodge, M. Marotti, Y. Rukazenkov, S. S. Ramalingam, F. Investigators, Osimertinib in Untreated EGFR-Mutated Advanced Non-Small-Cell Lung Cancer. *N Engl J Med* **378**, 113-125 (2018).
6. P. K. Brastianos, S. L. Carter, S. Santagata, D. P. Cahill, A. Taylor-Weiner, R. T. Jones, E. M. Van Allen, M. S. Lawrence, P. M. Horowitz, K. Cibulskis, K. L. Ligon, J. Tabernero, J. Seoane, E. Martinez-Saez, W. T. Curry, I. F. Dunn, S. H. Paek, S. H. Park, A. McKenna, A. Chevalier, M. Rosenberg, F. G. Barker, 2nd, C. M. Gill, P. Van Hummelen, A. R. Thorner, B. E. Johnson, M. P. Hoang, T. K. Choueiri, S. Signoretti, C. Sougnez, M. S. Rabin, N. U. Lin, E. P. Winer, A. Stemmer-Rachamimov, M. Meyerson, L. Garraway, S. Gabriel, E. S. Lander, R. Beroukhim, T. T. Batchelor, J. Baselga, D. N. Louis, G. Getz, W. C. Hahn, Genomic Characterization of Brain Metastases Reveals Branched Evolution and Potential Therapeutic Targets. *Cancer Discov* **5**, 1164-1177 (2015).
7. D. J. H. Shih, N. Nayyar, I. Bihun, I. Dagogo-Jack, C. M. Gill, E. Aquilanti, M. Bertalan, A. Kaplan, M. R. D'Andrea, U. Chukwueke, F. M. Ippen, C. Alvarez-Breckenridge, N. D. Camarda, M. Lastrapes, D. McCabe, B. Kuter, B. Kaufman, M. R. Strickland, J. C. Martinez-Gutierrez, D. Nagabhushan, M. De Sauvage, M. D. White, B. A. Castro, K. Hoang, A. Kaneb, E. D. Batchelor, S. H. Paek, S. H. Park, M. Martinez-Lage, A. S. Berghoff, P. Merrill, E. R. Gerstner, T. T. Batchelor, M. P. Frosch, R. P. Frazier, D. R. Borger, A. J. Iafrate, B. E. Johnson, S. Santagata, M. Preusser, D. P. Cahill, S. L. Carter, P. K. Brastianos, Genomic characterization of human brain metastases identifies drivers of metastatic lung adenocarcinoma. *Nat Genet* **52**, 371-377 (2020).
8. M. Singh, C. Venugopal, T. Tokar, K. R. Brown, N. McFarlane, D. Bakhshinyan, T. Vijayakumar, B. Manoranjan, S. Mahendram, P. Vora, M. Qazi, M. Dhillon, A. Tong, K. Durrer, N. Murty, R. Hallet, J. A. Hassell, D. R. Kaplan, J. C. Cutz, I. Jurisica, J. Moffat, S. K. Singh, RNAi screen identifies essential regulators of human brain metastasis-initiating cells. *Acta Neuropathol* **134**, 923-940 (2017).
9. D. X. Nguyen, A. C. Chiang, X. H. Zhang, J. Y. Kim, M. G. Kris, M. Ladanyi, W. L. Gerald, J. Massague, WNT/TCF signaling through LEF1 and HOXB9 mediates lung adenocarcinoma metastasis. *Cell* **138**, 51-62 (2009).
10. M. Singh, N. Garg, C. Venugopal, R. Hallett, T. Tokar, N. McFarlane, S. Mahendram, D. Bakhshinyan, B. Manoranjan, P. Vora, M. Qazi, C. C. Arpin, B. Page, S. Haftchenary, D. A. Rosa, P. S. Lai, R. F. Gomez-Biagi, A. M. Ali, A. Lewis, M. Geletu, N. K. Murty, J. A. Hassell, I. Jurisica, P. T. Gunning, S. K. Singh, STAT3 pathway regulates lung-derived brain metastasis initiating cell capacity through miR-21 activation. *Oncotarget* **6**, 27461-27477 (2015).
11. M. Valiente, A. C. Obenauf, X. Jin, Q. Chen, X. H. Zhang, D. J. Lee, J. E. Chaft, M. G. Kris, J. T. Huse, E. Brogi, J. Massague, Serpins promote cancer cell survival and vascular co-option in brain metastasis. *Cell* **156**, 1002-1016 (2014).
12. B. I. Bassey-Archibong, C. Rajendra Chokshi, N. Aghaei, A. M. Kieliszek, N. Tatari, D. McKenna, M. Singh, M. Kalpana Subapanditha, A. Parmar, D. Mobilio, N. Savage, F. Lam, T. Tokar, J. Provias, Y.

Lu, S. C. Chafe, C. Swanton, R. E. Hynds, C. Venugopal, S. K. Singh, An HLA-G/SPAG9/STAT3 axis promotes brain metastases. *Proc Natl Acad Sci U S A* **120**, e2205247120 (2023).

13. R. E. Hynds, A. Huebner, D. R. Pearce, M. S. Hill, A. U. Akarca, D. A. Moore, S. Ward, K. H. C. Gowers, T. Karasaki, M. Al Bakir, G. A. Wilson, O. Pich, C. Martinez-Ruiz, A. Hossain, S. P. Pearce, M. Sivakumar, A. Ben Aissa, E. Gronroos, D. Chandrasekharan, K. K. Kolluri, R. Towns, K. Wang, D. E. Cook, L. Bosshard-Carter, C. Naceur-Lombardelli, A. J. Rowan, S. Veeriah, K. Litchfield, P. A. J. Crosbie, C. Dive, S. A. Quezada, S. M. Janes, M. Jamal-Hanjani, T. Marafioti, T. R. consortium, N. McGranahan, C. Swanton, Representation of genomic intratumor heterogeneity in multi-region non-small cell lung cancer patient-derived xenograft models. *Nat Commun* **15**, 4653 (2024).
14. L. S. Qi, M. H. Larson, L. A. Gilbert, J. A. Doudna, J. S. Weissman, A. P. Arkin, W. A. Lim, Repurposing CRISPR as an RNA-guided platform for sequence-specific control of gene expression. *Cell* **152**, 1173-1183 (2013).
15. P. Mali, J. Aach, P. B. Stranges, K. M. Esvelt, M. Moosburner, S. Kosuri, L. Yang, G. M. Church, CAS9 transcriptional activators for target specificity screening and paired nickases for cooperative genome engineering. *Nat Biotechnol* **31**, 833-838 (2013).
16. K. R. Sanson, R. E. Hanna, M. Hegde, K. F. Donovan, C. Strand, M. E. Sullender, E. W. Vaimberg, A. Goodale, D. E. Root, F. Piccioni, J. G. Doench, Optimized libraries for CRISPR-Cas9 genetic screens with multiple modalities. *Nat Commun* **9**, 5416 (2018).
17. A. M. Kieliszek, D. Mobilio, B. I. Bassey-Archibong, J. W. Johnson, M. L. Piotrowski, E. D. de Araujo, A. Sedighi, N. Aghaei, L. Escudero, P. Ang, W. D. Gwynne, C. Zhang, A. Quaile, D. McKenna, M. Subapanditha, T. Tokar, M. Vaseem Shaikh, K. Zhai, S. C. Chafe, P. T. Gunning, J. R. Montenegro-Burke, C. Venugopal, J. Magolan, S. K. Singh, De novo GTP synthesis is a metabolic vulnerability for the interception of brain metastases. *Cell Rep Med* **5**, 101755 (2024).
18. A. Tsherniak, F. Vazquez, P. G. Montgomery, B. A. Weir, G. Kryukov, G. S. Cowley, S. Gill, W. F. Harrington, S. Pantel, J. M. Krill-Burger, R. M. Meyers, L. Ali, A. Goodale, Y. Lee, G. Jiang, J. Hsiao, W. F. J. Gerath, S. Howell, E. Merkel, M. Ghandi, L. A. Garraway, D. E. Root, T. R. Golub, J. S. Boehm, W. C. Hahn, Defining a Cancer Dependency Map. *Cell* **170**, 564-576 e516 (2017).
19. S. Wei, W. Liu, M. Xu, H. Qin, C. Liu, R. Zhang, S. Zhou, E. Li, Z. Liu, Q. Wang, Cathepsin F and Fibulin-1 as novel diagnostic biomarkers for brain metastasis of non-small cell lung cancer. *Br J Cancer* **126**, 1795-1805 (2022).
20. L. Sevenich, R. L. Bowman, S. D. Mason, D. F. Quail, F. Rapaport, B. T. Elie, E. Brogi, P. K. Brastianos, W. C. Hahn, L. J. Holsinger, J. Massague, C. S. Leslie, J. A. Joyce, Analysis of tumour- and stroma-supplied proteolytic networks reveals a brain-metastasis-promoting role for cathepsin S. *Nat Cell Biol* **16**, 876-888 (2014).
21. G. B. Ferraro, A. Ali, A. Luengo, D. P. Kodack, A. Deik, K. L. Abbott, D. Bezwada, L. Blanc, B. Prideaux, X. Jin, J. M. Posada, J. Chen, C. R. Chin, Z. Amoozgar, R. Ferreira, I. X. Chen, K. Naxerova, C. Ng, A. M. Westermark, M. Duquette, S. Roberge, N. I. Lindeman, C. A. Lyssiotis, J. Nielsen, D. E. Housman, D. G. Duda, E. Brachtel, T. R. Golub, L. C. Cantley, J. M. Asara, S. M. Davidson, D. Fukumura, V. A. Dartois, C. B. Clish, R. K. Jain, M. G. Vander Heiden, Fatty Acid Synthesis Is Required for Breast Cancer Brain Metastasis. *Nat Cancer* **2**, 414-428 (2021).
22. X. Jin, Z. Demere, K. Nair, A. Ali, G. B. Ferraro, T. Natoli, A. Deik, L. Petronio, A. A. Tang, C. Zhu, L. Wang, D. Rosenberg, V. Mangena, J. Roth, K. Chung, R. K. Jain, C. B. Clish, M. G. Vander Heiden, T. R. Golub, A metastasis map of human cancer cell lines. *Nature* **588**, 331-336 (2020).
23. S. M. Nolte, C. Venugopal, N. McFarlane, O. Morozova, R. M. Hallett, E. O'Farrell, B. Manoranjan, N. K. Murty, P. Klurfan, E. Kachur, J. P. Provias, F. Farrokhyar, J. A. Hassell, M. Marra, S. K. Singh, A cancer stem cell model for studying brain metastases from primary lung cancer. *J Natl Cancer Inst* **105**, 551-562 (2013).

24. M. Singh, C. Venugopal, T. Tokar, N. McFarlane, M. K. Subapanditha, M. Qazi, D. Bakhshinyan, P. Vora, N. K. Murty, I. Jurisica, S. K. Singh, Therapeutic Targeting of the Premetastatic Stage in Human Lung-to-Brain Metastasis. *Cancer Res* **78**, 5124-5134 (2018).
25. S. K. Singh, C. Hawkins, I. D. Clarke, J. A. Squire, J. Bayani, T. Hide, R. M. Henkelman, M. D. Cusimano, P. B. Dirks, Identification of human brain tumour initiating cells. *Nature* **432**, 396-401 (2004).
26. K. E. Coleman, M. Bekes, J. R. Chapman, S. B. Crist, M. J. Jones, B. M. Ueberheide, T. T. Huang, SENP8 limits aberrant neddylation of NEDD8 pathway components to promote cullin-RING ubiquitin ligase function. *Elife* **6**, (2017).
27. J. A. Hellyer, H. Stehr, M. Das, S. K. Padda, K. Ramchandran, J. W. Neal, M. Diehn, H. A. Wakelee, Impact of KEAP1/NFE2L2/CUL3 mutations on duration of response to EGFR tyrosine kinase inhibitors in EGFR mutated non-small cell lung cancer. *Lung Cancer* **134**, 42-45 (2019).
28. K. Zhai, Z. Huang, Q. Huang, W. Tao, X. Fang, A. Zhang, X. Li, G. R. Stark, T. A. Hamilton, S. Bao, Pharmacological inhibition of BACE1 suppresses glioblastoma growth by stimulating macrophage phagocytosis of tumor cells. *Nat Cancer* **2**, 1136-1151 (2021).
29. A. Naidu, B. Silverglate, M. Silverglate, G. T. Grossberg, Safety concerns associated with BACE1 inhibitors - past, present, and future. *Expert Opin Drug Saf*, 1-6 (2025).
30. Q. Zhang, R. Abdo, C. Iosef, T. Kaneko, M. Cecchini, V. K. Han, S. S. Li, The spatial transcriptomic landscape of non-small cell lung cancer brain metastasis. *Nat Commun* **13**, 5983 (2022).
31. M. E. Kennedy, A. W. Stamford, X. Chen, K. Cox, J. N. Cumming, M. F. Dockendorf, M. Egan, L. Ereshefsky, R. A. Hodgson, L. A. Hyde, S. Jhee, H. J. Kleijn, R. Kuvelkar, W. Li, B. A. Mattson, H. Mei, J. Palcza, J. D. Scott, M. Tanen, M. D. Troyer, J. L. Tseng, J. A. Stone, E. M. Parker, M. S. Forman, The BACE1 inhibitor verubecestat (MK-8931) reduces CNS beta-amyloid in animal models and in Alzheimer's disease patients. *Sci Transl Med* **8**, 363ra150 (2016).
32. M. F. Clarke, J. E. Dick, P. B. Dirks, C. J. Eaves, C. H. Jamieson, D. L. Jones, J. Visvader, I. L. Weissman, G. M. Wahl, Cancer stem cells--perspectives on current status and future directions: AACR Workshop on cancer stem cells. *Cancer Res* **66**, 9339-9344 (2006).
33. K. Kleffman, G. Levinson, I. V. L. Rose, L. M. Blumenberg, S. A. A. Shadaloey, A. Dhabaria, E. Wong, F. Galan-Echevarria, A. Karz, D. Argibay, R. Von Itter, A. Floristan, G. Baptiste, N. M. Eskow, J. A. Tranos, J. Chen, Y. S. d. M. E. C. Vega, M. Call, R. Rogers, G. Jour, Y. Z. Wadghiri, I. Osman, Y. M. Li, P. Mathews, R. B. DeMattos, B. Ueberheide, K. V. Ruggles, S. A. Liddelow, R. J. Schneider, E. Hernando, Melanoma-Secreted Amyloid Beta Suppresses Neuroinflammation and Promotes Brain Metastasis. *Cancer Discov* **12**, 1314-1335 (2022).
34. Y. J. Guo, W. W. Pan, S. B. Liu, Z. F. Shen, Y. Xu, L. L. Hu, ERK/MAPK signalling pathway and tumorigenesis. *Exp Ther Med* **19**, 1997-2007 (2020).
35. S. V. Sharma, D. W. Bell, J. Settleman, D. A. Haber, Epidermal growth factor receptor mutations in lung cancer. *Nat Rev Cancer* **7**, 169-181 (2007).
36. O. Soderberg, M. Gullberg, M. Jarvius, K. Ridderstrale, K. J. Leuchowius, J. Jarvius, K. Wester, P. Hydbring, F. Bahram, L. G. Larsson, U. Landegren, Direct observation of individual endogenous protein complexes in situ by proximity ligation. *Nat Methods* **3**, 995-1000 (2006).
37. A. Doucet, C. M. Overall, Amino-Terminal Oriented Mass Spectrometry of Substrates (ATOMS) N-terminal sequencing of proteins and proteolytic cleavage sites by quantitative mass spectrometry. *Methods Enzymol* **501**, 275-293 (2011).
38. R. Yan, R. Vassar, Targeting the beta secretase BACE1 for Alzheimer's disease therapy. *Lancet Neurol* **13**, 319-329 (2014).
39. M. Forman, J. Palcza, J. Tseng, J. A. Stone, B. Walker, D. Swearingen, M. D. Troyer, M. F. Dockendorf, Safety, Tolerability, and Pharmacokinetics of the beta-Site Amyloid Precursor

Protein-Cleaving Enzyme 1 Inhibitor Verubecestat (MK-8931) in Healthy Elderly Male and Female Subjects. *Clin Transl Sci* **12**, 545-555 (2019).
40. F. Skoulidis, J. V. Heymach, Co-occurring genomic alterations in non-small-cell lung cancer biology and therapy. *Nat Rev Cancer* **19**, 495-509 (2019).
41. H. Ogiso, R. Ishitani, O. Nureki, S. Fukai, M. Yamanaka, J. H. Kim, K. Saito, A. Sakamoto, M. Inoue, M. Shirouzu, S. Yokoyama, Crystal structure of the complex of human epidermal growth factor and receptor extracellular domains. *Cell* **110**, 775-787 (2002).
42. G. Lamberti, A. Aizer, B. Ricciuti, J. V. Alessi, F. Pecci, S. C. Tseng, L. M. Sholl, M. Nishino, M. M. Awad, Incidence of Brain Metastases and Preliminary Evidence of Intracranial Activity With Sotorasib in Patients With KRAS(G12C)-Mutant Non-Small-Cell Lung Cancer. *JCO Precis Oncol* **7**, e2200621 (2023).
43. C. M. Ardito, B. M. Gruner, K. K. Takeuchi, C. Lubeseder-Martellato, N. Teichmann, P. K. Mazur, K. E. Delgiorno, E. S. Carpenter, C. J. Halbrook, J. C. Hall, D. Pal, T. Briel, A. Herner, M. Trajkovic-Arsic, B. Sipos, G. Y. Liou, P. Storz, N. R. Murray, D. W. Threadgill, M. Sibilia, M. K. Washington, C. L. Wilson, R. M. Schmid, E. W. Raines, H. C. Crawford, J. T. Siveke, EGF receptor is required for KRAS-induced pancreatic tumorigenesis. *Cancer Cell* **22**, 304-317 (2012).
44. C. Galaxy, The Galaxy platform for accessible, reproducible, and collaborative data analyses: 2024 update. *Nucleic Acids Res* **52**, W83-W94 (2024).
45. A. Ianevski, A. K. Giri, T. Aittokallio, SynergyFinder 3.0: an interactive analysis and consensus interpretation of multi-drug synergies across multiple samples. *Nucleic Acids Res* **50**, W739-W743 (2022).
46. A. M. K. Law, J. X. M. Yin, L. Castillo, A. I. J. Young, C. Piggin, S. Rogers, C. E. Caldon, A. Burgess, E. K. A. Millar, S. A. O'Toole, D. Gallego-Ortega, C. J. Ormandy, S. R. Oakes, Andy's Algorithms: new automated digital image analysis pipelines for FIJI. *Sci Rep* **7**, 15717 (2017).
47. B. Li, C. N. Dewey, RSEM: accurate transcript quantification from RNA-Seq data with or without a reference genome. *BMC Bioinformatics* **12**, 323 (2011).
48. C. Martinez-Ruiz, J. R. M. Black, C. Puttick, M. S. Hill, J. Demeulemeester, E. Larose Cadieux, K. Thol, T. P. Jones, S. Veeriah, C. Naceur-Lombardelli, A. Toncheva, P. Prymas, A. Rowan, S. Ward, L. Cubitt, F. Athanasopoulou, O. Pich, T. Karasaki, D. A. Moore, R. Salgado, E. Colliver, C. Castignani, M. Dietzen, A. Huebner, M. Al Bakir, M. Tanic, T. B. K. Watkins, E. L. Lim, A. M. Al-Rashed, D. Lang, J. Clements, D. E. Cook, R. Rosenthal, G. A. Wilson, A. M. Frankell, S. de Carne Trecesson, P. East, N. Kanu, K. Litchfield, N. J. Birkbak, A. Hackshaw, S. Beck, P. Van Loo, M. Jamal-Hanjani, T. R. Consortium, C. Swanton, N. McGranahan, Genomic-transcriptomic evolution in lung cancer and metastasis. *Nature* **616**, 543-552 (2023).
49. A. M. Frankell, M. Dietzen, M. Al Bakir, E. L. Lim, T. Karasaki, S. Ward, S. Veeriah, E. Colliver, A. Huebner, A. Bunkum, M. S. Hill, K. Grigoriadis, D. A. Moore, J. R. M. Black, W. K. Liu, K. Thol, O. Pich, T. B. K. Watkins, C. Naceur-Lombardelli, D. E. Cook, R. Salgado, G. A. Wilson, C. Bailey, M. Angelova, R. Bentham, C. Martinez-Ruiz, C. Abbosh, A. G. Nicholson, J. Le Quesne, D. Biswas, R. Rosenthal, C. Puttick, S. Hessey, C. Lee, P. Prymas, A. Toncheva, J. Smith, W. Xing, J. Nicod, G. Price, K. M. Kerr, B. Naidu, G. Middleton, K. G. Blyth, D. A. Fennell, M. D. Forster, S. M. Lee, M. Falzon, M. Hewish, M. J. Shackcloth, E. Lim, S. Benafif, P. Russell, E. Boleti, M. G. Krebs, J. F. Lester, D. Papadatos-Pastos, T. Ahmad, R. M. Thakrar, D. Lawrence, N. Navani, S. M. Janes, C. Dive, F. H. Blackhall, Y. Summers, J. Cave, T. Marafioti, J. Herrero, S. A. Quezada, K. S. Peggs, R. F. Schwarz, P. Van Loo, D. M. Miedema, N. J. Birkbak, C. T. Hiley, A. Hackshaw, S. Zaccaria, T. R. Consortium, M. Jamal-Hanjani, N. McGranahan, C. Swanton, The evolution of lung cancer and impact of subclonal selection in TRACERx. *Nature* **616**, 525-533 (2023).
50. S. A. Forbes, D. Beare, P. Gunasekaran, K. Leung, N. Bindal, H. Boutselakis, M. Ding, S. Bamford, C. Cole, S. Ward, C. Y. Kok, M. Jia, T. De, J. W. Teague, M. R. Stratton, U. McDermott, P. J. Campbell,

COSMIC: exploring the world's knowledge of somatic mutations in human cancer. *Nucleic Acids Res* **43**, D805-811 (2015).
51. X. Wang, H. Bai, J. Zhang, Z. Wang, J. Duan, H. Cai, Z. Cao, Q. Lin, X. Ding, Y. Sun, W. Zhang, X. Xu, H. Chen, D. Zhang, X. Feng, J. Wan, J. Zhang, J. He, J. Wang, Genetic Intratumor Heterogeneity Remodels the Immune Microenvironment and Induces Immune Evasion in Brain Metastasis of Lung Cancer. *J Thorac Oncol* **19**, 252-272 (2024).

Acknowledgments: We would like to thank the Brain Tumor and Neuro-Oncology Centers at the Cleveland Clinic and Hamilton Health Sciences for providing surgical specimens for this study. We greatly appreciate the help provided by Ms. Mary McGraw from the Brain Tumor Bank at Cleveland Clinic. We thank the Flow Cytometry Core, Imaging Core, and Central Cell Services at Cleveland Clinic Lerner Research Institute for their assistance. We thank members of the lung TRACERx consortium whose study enabled the derivation of patient-derived xenografts and cell lines that were used in this study.

Funding: This study was supported by funds from the Department of Surgery at McMaster University, a Canadian Cancer Society Innovation to Impact grant (i2I16-1), the Boris Family Fund for Brain Metastasis Research and the Canadian Institutes of Health Research (S.K.S), the Cleveland Clinic Foundation and Lerner Research Institute lung cancer research grant (S.B.), a Sir Henry Wellcome Fellowship (Wellcome Trust; WT209199/Z/17/Z; R.E.H), and by the Cancer Research UK Lung Cancer Centre of Excellence (C.S). The TRACERx patient-derived xenografts and cell line derivations were supported by the Francis Crick Institute which receives its core funding from Cancer Research UK (CC2041), the UK Medical Research Council (CC2041), and the Wellcome Trust (CC2041). This work utilized an IVIS system (Spectrum CT) that was purchased with NIH SIG grants 1S10RR031536-01 and S10OD018205.

Author Contributions:

Conceptualization: S.C.C, K.Z, N.A, C.V, S.K.S, S.B; Methodology: S.C.C, K.Z, N.A, P.M, Z.H, D.M, D.Y, Y.S, S.G, F.C.L, R. A, B.B.A, Q.Z, S.S.C.L, A.D; Investigation: S.C.C, K.Z, N.A, P.M, Z.H, K.R.B, D.M, D.Y, Y.S, S.G, D.M, Z.A, A.M.K, R.E.H, F.C.L, L.E, Q.H, J.L, P.A, A.A, S.C, E.A, S.S, B.B, J.K; Formal analysis: S.C.C, K.Z, N.A, P.M, Z.H, K.R.B, D.M, D.Y, Y.S, S.G, R.E.H, F.C.L, L.E, C.V, J-Q,L, J-C.C, Q.Z, A.D; Data curation: S.C.C, K.Z, P.M, K.R.B, D.Y, C.V, Q.Z; Visualization: S.C.C, K.Z, N.A, P.M, Z.H, D.M; Writing original draft: S.C.C, K.Z; Writing, review, and editing: S.C.C, K.Z, N.A, P.M, D.M, A.M.K, A.H, B. B.A, R.E.H, C.V, C.S, S.B, S.K.S; Supervision: S.C.C, K.Z, S.S.C.L, C.V, A.D, J.M, C.S, S.B, S.K.S; Funding acquisition: C.S, S.B, S.K.S;

Competing interests: S.B. and K.Z are listed as inventors in an issued patent application (US patent# 11559528) related to this study. Other authors declare no competing interests relevant to the current study.

Data and materials availability: All data associated with this study are in the paper or the supplementary materials. All sequencing and proteomic data have been deposited into their appropriate databases. All FASTQ files from the CRISPR screen have been deposited in the Gene Expression Omnibus (GEO) under accession # GSE237446. All proteomic data has been deposited in the PRIDE database under accession # PXD060790. All requests for reagents will be fulfilled by SKS or SB following completion of material transfer agreements with McMaster University (SKS) or the Cleveland Clinic (SB).

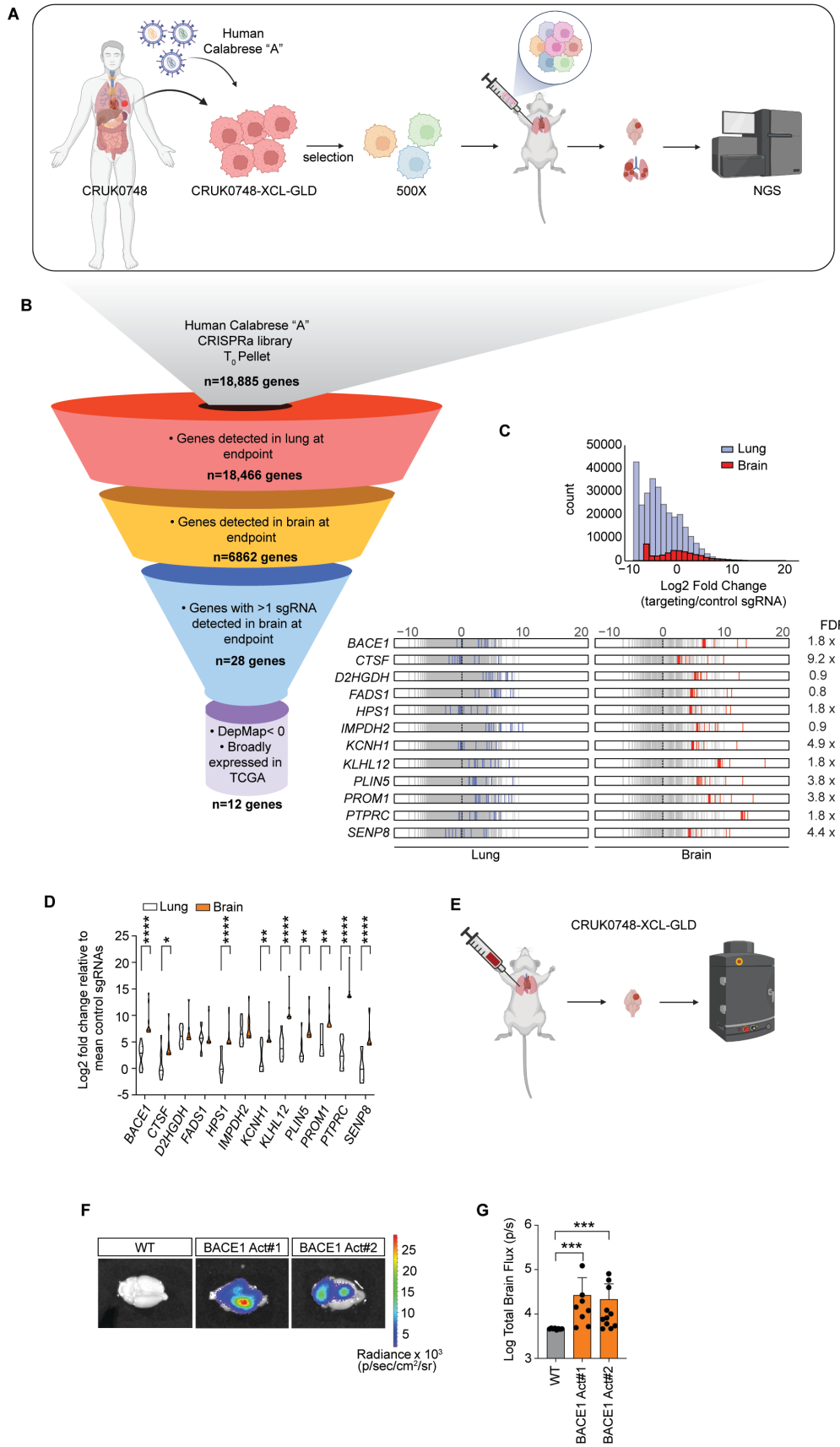
A
Human Calabrese "A"
CRUK0748
CRUK0748-XCL-GLD
selection
500X
NGS
B
Human Calabrese "A" CRISPRa library T0 Pellet
n=18,885 genes
• Genes detected in lung at endpoint
n=18,466 genes
• Genes detected in brain at endpoint
n=6862 genes
• Genes with >1 sgRNA detected in brain at endpoint
n=28 genes
• DepMap< 0
• Broadly expressed in TCGA
n=12 genes
C
Lung
Brain
count
Log2 Fold Change (targeting/control sgRNA)
FDR
BACE1 1.8 x 10-5
CTSF 9.2 x 10-3
D2HGDH 0.9
FADS1 0.8
HPS1 1.8 x 10-5
IMPDH2 0.9
KCNH1 4.9 x 10-3
KLHL12 1.8 x 10-5
PLIN5 3.8 x 10-3
PROM1 3.8 x 10-3
PTPRC 1.8 x 10-5
SENP8 4.4 x 10-4
Lung
Brain
D
Lung
Brain
Log2 fold change relative to mean control sgRNAs
BACE1
CTSF
D2HGDH
FADS1
HPS1
IMPDH2
KCNH1
KLHL12
PLIN5
PROM1
PTPRC
SENP8
E
CRUK0748-XCL-GLD
F
WT
BACE1 Act#1
BACE1 Act#2
Radiance x 10³ (p/sec/cm²/sr)
G
Log Total Brain Flux (p/s)
WT
BACE1 Act#1
BACE1 Act#2

Fig. 1. *In vivo* CRISPR activation screen identifies *BACE1* drives LUAD brain metastasis. (**A**) *In vivo* CRISPR activation screen schematic. NGS – next generation sequencing. (**B**) Schematic depicting our screen hit prioritization strategy. (**C**) Distribution and rug plots displaying $\log_2$ fold change of normalized sgRNA read counts (blue ticks – lungs, red ticks – brains) from individual lungs and brains relative to the mean of the control sgRNAs from the respective tissue. The distribution of the control sgRNAs is displayed as gray lines. Dotted line is $\log_2$ fold change of 0. (**D**) Violin plot depicting the relative enrichment of the sgRNAs of the indicated genes in the brain or lung as $\log_2$ FC compared to the control sgRNAs of the indicated tissue (n=12, one experiment). (**E**) Experimental scheme for orthotopic (intralung) implantation of CRISPR-activated *BACE1* CRUK0748-XCL-GLD cells. (**F**) *Ex vivo* bioluminescent images of brains from mice in the indicated groups at endpoint (n=10 per group, one experiment). (**G**) Quantification of the total flux of the *ex vivo* brain bioluminescent images in (F). Data in (C) were analyzed by one-sided Wilcoxon rank sum test with Benjamini-Holchberg correction (FDR). Data in (D) were analyzed by two-way ANOVA. Data in (G) were analyzed by Mann-Whitney U test. *P<0.05, **P<0.01, ***P<0.001, ****P<0.0001

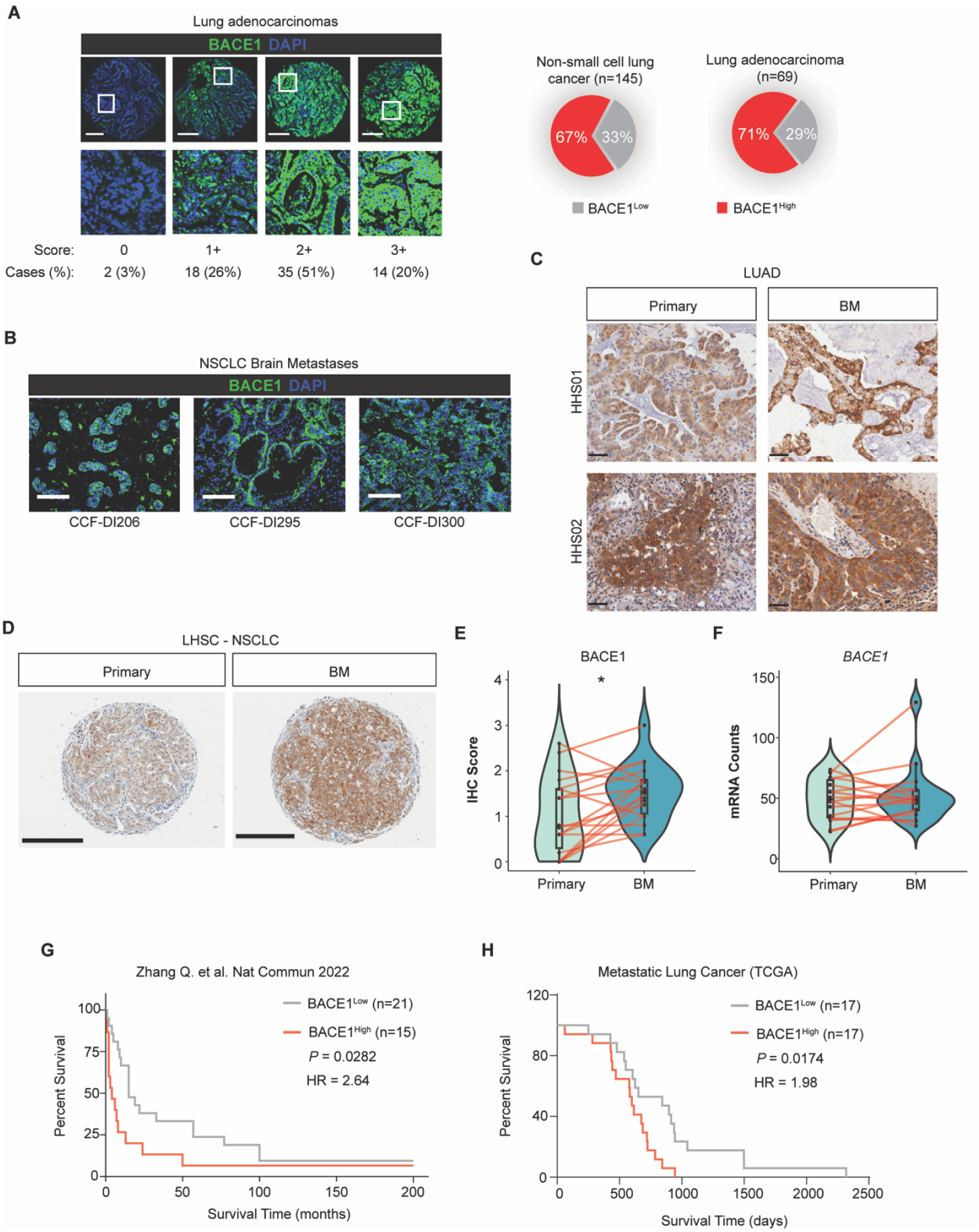

Fig. 2. BACE1 is expressed in LUAD brain metastasis and is associated with worse prognosis. (**A**) (*Left*) Lung cancer tumor microarray (*n*=145) including lung

adenocarcinomas (*n*=69) stained for BACE1. Green – BACE1, Blue – DAPI (nuclei). (*Right*) Pie charts indicating the proportion of tumors staining high or low for BACE1 in all non-small cell lung cancers (left) or in lung adenocarcinomas (right). Scale bar = 250 μm. (**B**) Immunohistochemical staining of brain metastases from patients with LUAD for BACE1. Colored as in (A). Scale bar = 250 μm. (**C**) Immunohistochemical staining of BACE1 in primary LUAD and matched brain metastases from Hamilton Health Sciences. Scale bar = 50 μm. (**D**) Immunohistochemical staining of BACE1 in the primary NSCLC and matched brain metastases TMA from London Health Sciences Centre (LHSC). Scale bar = 300 μm. **(E)** Violin plot depicting quantitation of BACE1 staining in (D) (*n*=21). **(F)** Violin plot depicting mRNA counts from GeoMx analyses of the samples in (D). **(G)** Kaplan-Meier curve depicting survival proportions for patients from the LHSC cohort according to BACE1 expression. **(H)** Kaplan-Meier curve depicting survival proportions for patients from the TCGA with LUAD brain metastases stratified according to median *BACE1* expression. Hazard ratio determined using multivariate analysis with Cox Proportional Hazards mode (G,H). Data in (E) was analyzed by t test. Data in (H) was analyzed by Log-rank test. *P<0.05

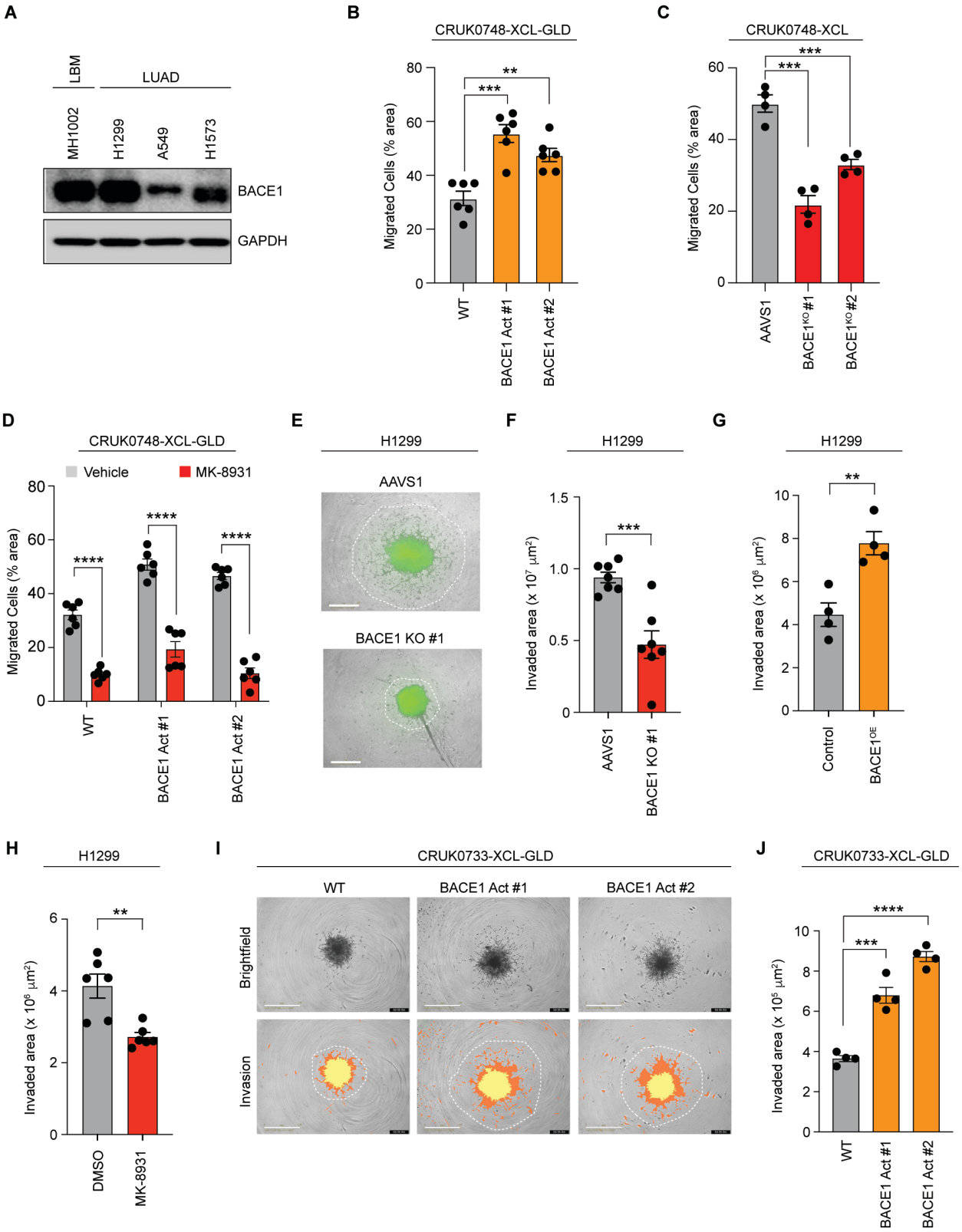
A
LBM
LUAD
MH1002
H1299
A549
H1573
BACE1
GAPDH
B
CRUK0748-XCL-GLD
Migrated Cells (% area)
WT
BACE1 Act #1
BACE1 Act #2
C
CRUK0748-XCL
AAVS1
BACE1KO #1
BACE1KO #2
D
CRUK0748-XCL-GLD
Vehicle
MK-8931
E
H1299
AAVS1
BACE1 KO #1
F
H1299
Invaded area (x 10⁷ µm²)
G
H1299
Invaded area (x 10⁶ µm²)
Control
BACE1OE
H
H1299
Invaded area (x 10⁶ µm²)
DMSO
MK-8931
I
CRUK0733-XCL-GLD
Brightfield
Invasion
J
CRUK0733-XCL-GLD
Invaded area (x 10⁵ µm²)

769

Fig. 3. BACE1 increases the migratory and invasive capacity of primary LUAD cells. (**A**) Western blot analysis of BACE1 expression in a panel of non-small cell lung cancer and lung-to-brain metastasis (LBM) lines. (**B**) Quantification of the migrated cell area of CRUK0748-XCL-GLD cells following BACE1 activation (*n*=6, *N*=3). (**C**) Quantification of the migrated cell area of *BACE1*^{KO} CRUK0748-XCL cells (*n*=4, *N*=3). (**D**) Quantification of migrated cell area of MK-8931 (10 μM) treated CRUK0748-XCL-GLD cells (*n*=6, *N*=3). (**E**) Representative micrographs depicting spheroid invasion of BACE1^{KO} H1299^{GFP} after 7 days in Matrigel™. White boundaries indicate extent of invasion for the indicated cell lines. Scale bar = 800 μm. (**F**) Quantification of the invaded area of the indicated cell lines in (E) quantified using ImageJ (*n*=7, *N*=2). (**G**) Quantification of H1299^{GFP} invasion in a spheroid invasion model following overexpression of *BACE1* (*n*=4, *N*=2). (**H**) Quantification of H1299^{GFP} invasion in a spheroid invasion model following treatment with MK-8931 (50 μM) for 7 days (*n*=6, *N*=2). (**I**) Representative micrographs depicting spheroid invasion of CRISPR-activated *BACE1* CRUK0733-XCL-GLD cells after 80 hours in Matrigel™. Invasion images illustrate the quantification mask from the Incucyte® spheroid software module utilized to quantify the extent of invasion. Yellow marks the growth of the sphere; orange and white mark the extent of invasion. Scale bar = 1 mm. (**J**) Quantification of invasion in (I) (*n*=4, *N*=2). Bars represent the mean number of migrated cells or invaded area ± SEM. Data in (B), (C), (F), (G), (H) and (J) was analyzed by t test. Data in (D) was analyzed by two-way ANOVA with Sidak's multiple comparisons test. ***P*<0.01, ****P*<0.001*****P*<0.0001.

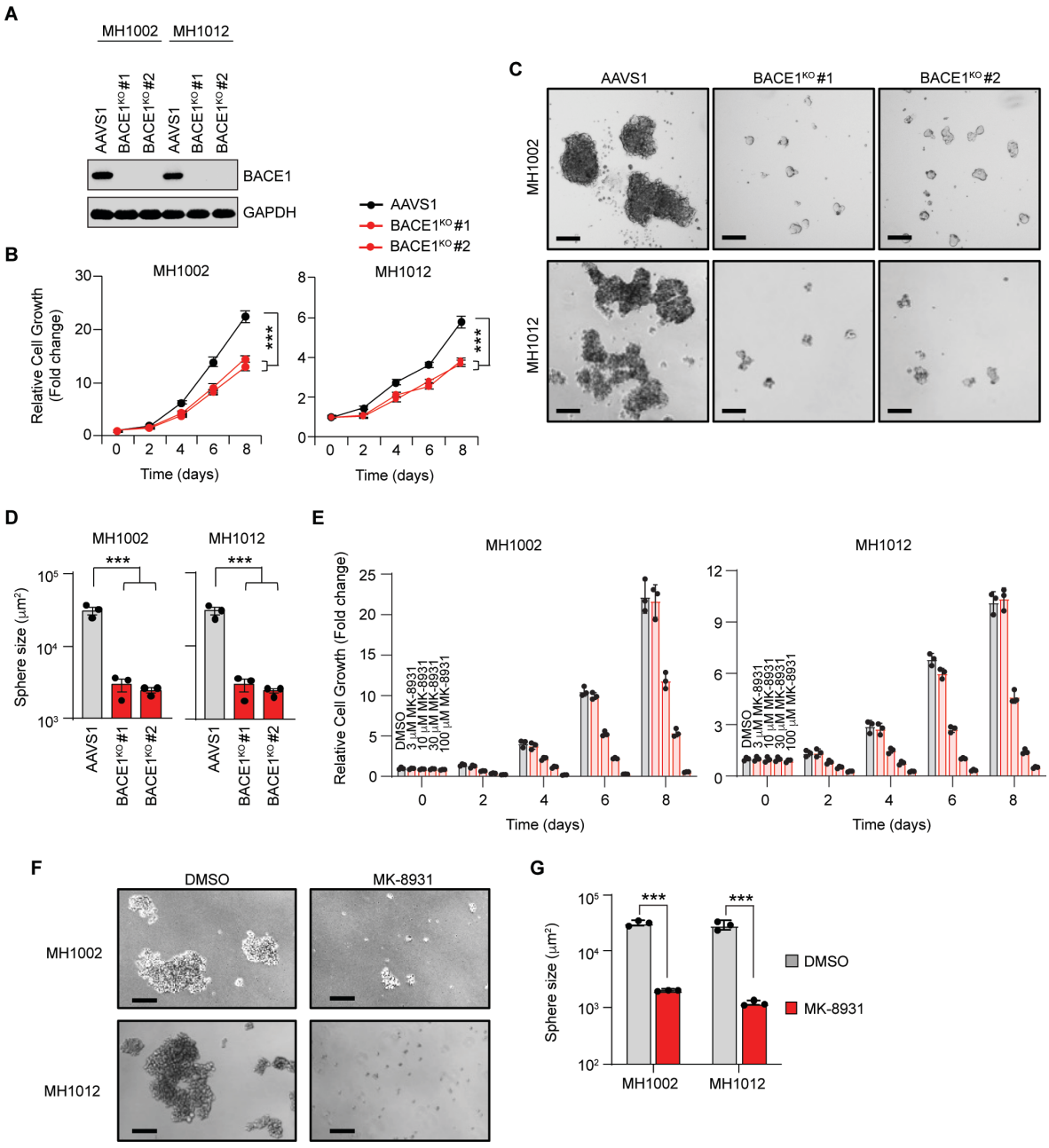

Fig. 4. BACE1 is required for the proliferation and self-renewal capacity of LUAD brain metastases. (**A**) Western blot analysis of BACE1 expression in control (AAVS1^{KO}) or BACE1^{KO} MH1002 cells. (**B**) Proliferation of BACE1^{KO} MH1002 (left) and MH1012 (right) cells (*n*=3, *N*=3). (**C**) Micrographs depicting the sphere formation capacity of BACE1^{KO} MH1002 (Top) and MH1012 (Bottom) cells. Scale bar = 200 μm. (**D**) Quantification of sphere size for the indicated cell lines in (C) (*n*=3, *N*=3). (**E**) Cell

proliferation of the indicated cell lines in response to MK-8931 at the indicated doses after 72 hours (*n*=3, *N*=3). (**F**) Micrographs depicting the sphere formation capacity of the indicated cell lines in response to 50 μM MK-8931 treatment for 96 hours. Spheres were allowed to form for seven days (*n*=3, *N*=3). Scale bar = 200 μm. (**G**) Quantification of sphere size from the images in (F). Bars indicate mean ± SEM. Data in (B) were analyzed by two-way ANOVA with Tukey's multiple comparisons test. Data in (D) and (G) were analyzed by t test. ***$p<0.001$.

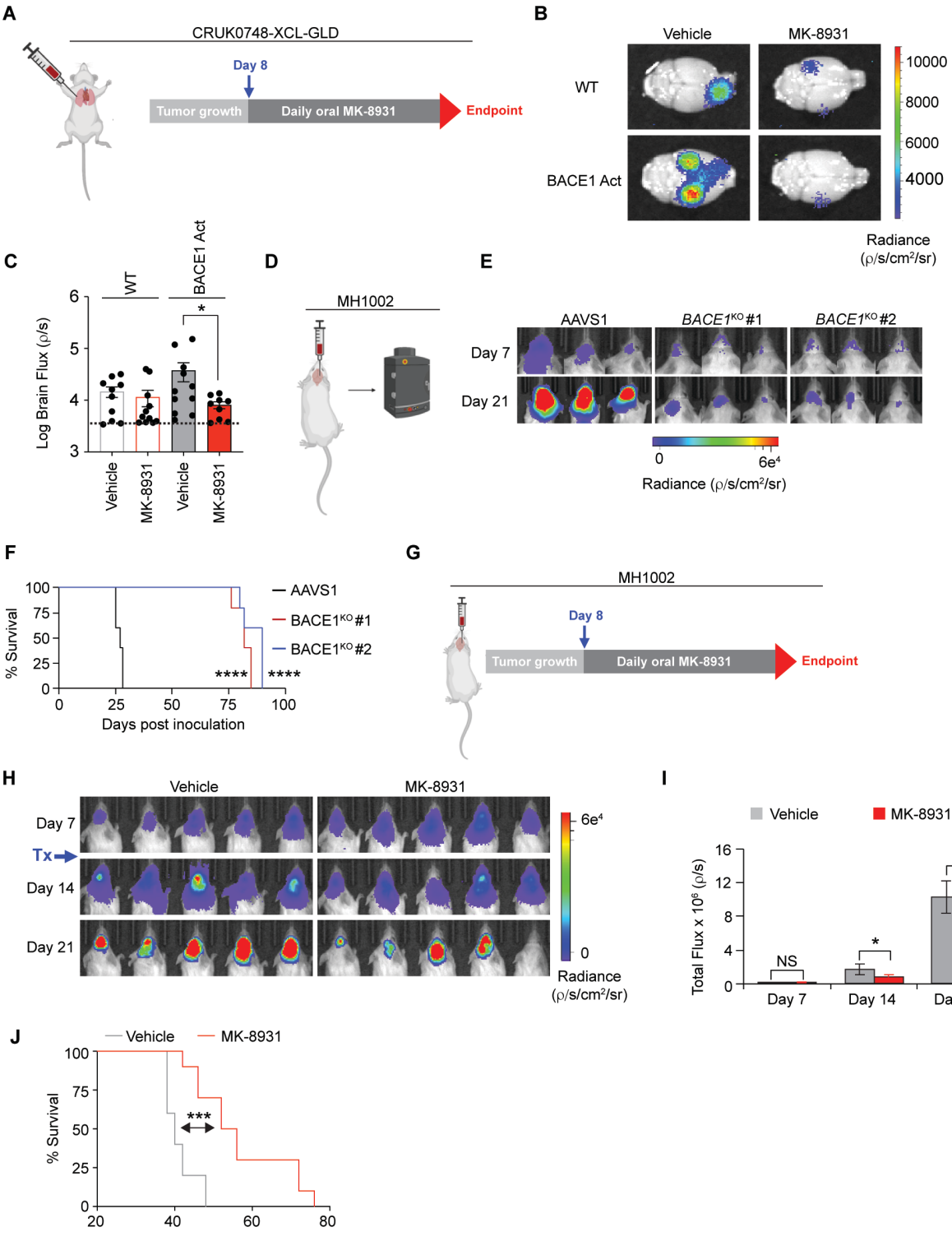

Fig. 5. Perturbing BACE1 expression or activity blocks the formation of LUAD brain metastases. (**A**) Experimental scheme for orthotopic injection (intralung) of CRISPR-activated *BACE1* CRUK0748-XCL-GLD cells treated daily by oral gavage with 30 mg/kg

MK-8931 for 21 days. (**B**) Representative *ex vivo* bioluminescent images of brains from the indicated groups. (**C**) Quantification of the total brain flux for all mice of the indicated groups. Dashed line indicates baseline luminescence (*n*=9-11 per group, one experiment). BACE1-Act Vehicle vs WT Vehicle *P*= 0.23. (**D**) Experimental scheme for intracranial injection of $BACE1^{KO}$ MH1002 cells. (**E**) Longitudinal bioluminescent images of representative mice from the indicated groups (*n*=5 per group, one experiment). (**F**) Kaplan-Meier curve depicting the survival times of mice across the indicated groups. (**G**) Experimental scheme for intracranial injection of MH1002 cells treated daily by oral gavage with 30 mg/kg MK-8931 for 21 days. (**H**) Longitudinal bioluminescent images of representative mice from the indicated groups. (**I**) Quantification of the total brain bioluminescent flux for the indicated groups over time (*n*=8 per group, one experiment). (**J**) Kaplan-Meier curve depicting the survival times of the mice across the indicated groups. Bars indicate mean ± SEM. Data in (C) were analyzed by Mann-Whitney U test. Data in (F) and (J) were analyzed by log-rank test. Data in (I) were analyzed by t test. **P*<0.05, ****p*<0.001, *****P*<0.0001.

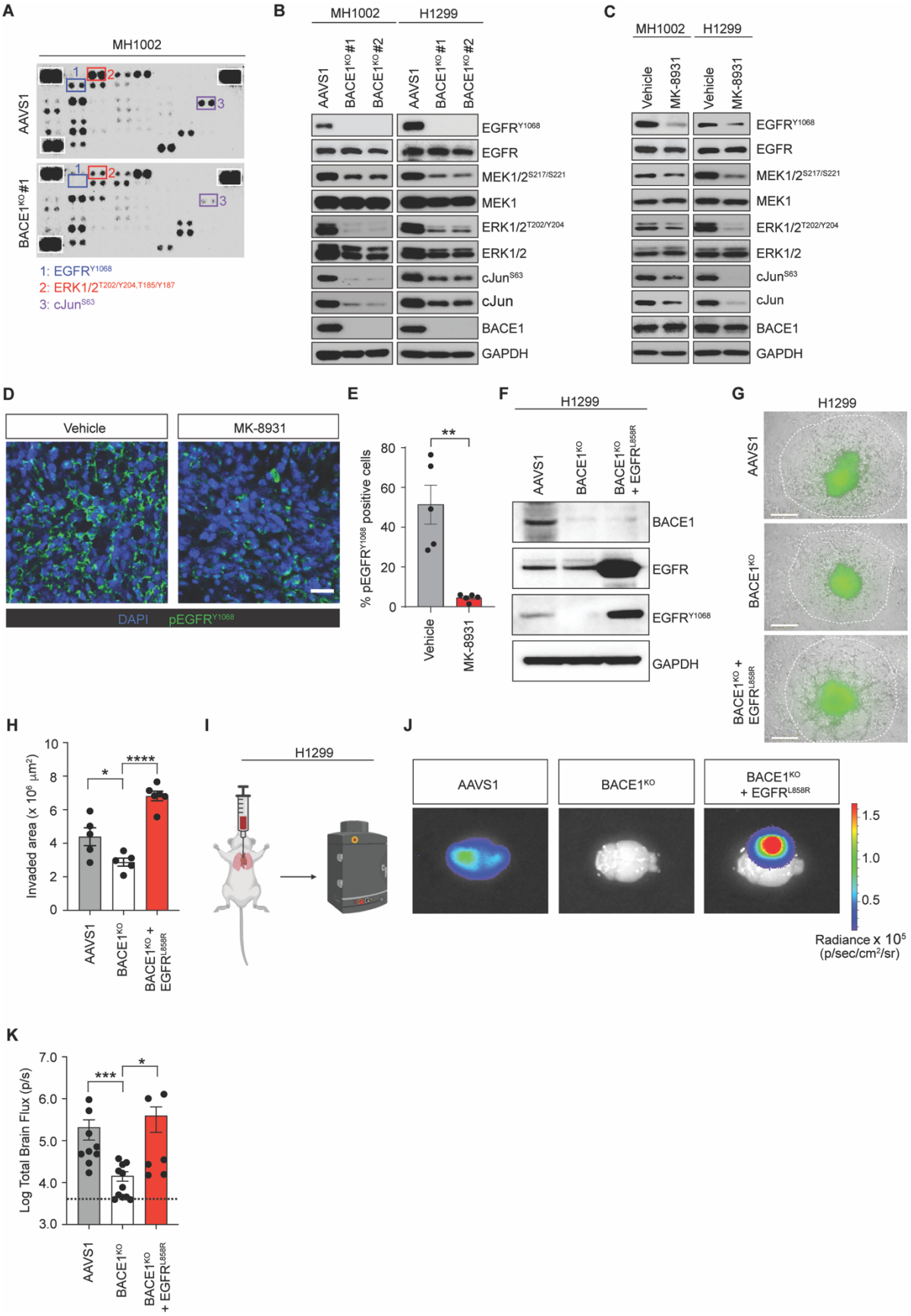
A
MH1002
AAVS1
BACE1KO#1
1: EGFRY1068
2: ERK1/2T202/Y204,T185/Y187
3: cJunS63
B
MH1002
H1299
AAVS1
BACE1KO#1
BACE1KO#2
EGFRY1068
EGFR
MEK1/2S217/S221
MEK1
ERK1/2T202/Y204
ERK1/2
cJunS63
cJun
BACE1
GAPDH
C
MH1002
H1299
Vehicle
MK-8931
D
Vehicle
MK-8931
DAPI
pEGFRY1068
E
% pEGFRY1068 positive cells
F
H1299
BACE1KO + EGFRL858R
G
H1299
H
Invaded area (x 10^6 µm^2)
I
J
Radiance x 10^5 (p/sec/cm^2/sr)
K
Log Total Brain Flux (p/s)

876

Fig. 6. BACE1 activity is required for EGFR activation. (**A**) Human Proteome Profiler™ phospho-kinase antibody array in lysates from *BACE1*^{KO} cells. (**B**) Western blot analysis of the indicated proteins in lysates from *BACE1*^{KO} cells (*N*=2). (**C**) Western blot analysis of the indicated proteins in lysates from cells treated with 30 μM MK-8931 for 72 hours (*N*=2). (**D**) Representative micrographs depicting EGFR^{Y1068} staining in MH1002 tumors treated with vehicle or 30 mg/kg MK-8931 (*n*=5 per group, one experiment). Green – EGFR^{Y1068}; Blue – DAPI. Scale bar = 30 μm. (**E**) Quantification of proportions of EGFR^{Y1068} positivity in MH1002 tumors in response to vehicle or MK-8931 treatment. (**F**) Western blot analysis of H1299^{GFP} BACE1^{KO} cells restored with EGFR^{L858R} for the indicated proteins (*N*=2). (**G**) Representative micrographs depicting spheroid invasion of BACE1^{KO} H1299^{GFP} with or without EGFR^{L858R} expression after 7 days in Matrigel™. White boundaries indicate extent of invasion for the indicated cell lines. Scale bar = 800 μm. (**H**) Quantification of the invaded area of the indicated cell lines in (G) (*n*=5-6, *N*=2). (**I**) Schematic for intracardiac injection of H1299$^{GFP\text{-}Luc}$ control, BACE1^{KO} or BACE1$^{KO\ +\ EGFRL858R}$ cells. (**J**) Representative *ex vivo* BLI images of brains from the indicated groups (*n*=9-10 per group). (**K**) Quantification of total brain flux from individual mice from the indicated groups. Bars represent mean ± SEM. Data in (E) and (H) were analyzed by t test. Data in (K) were analyzed by Mann-Whitney U test. **P*<0.05, ***P*<0.01, ****P*<0.001, *****P*<0.0001.

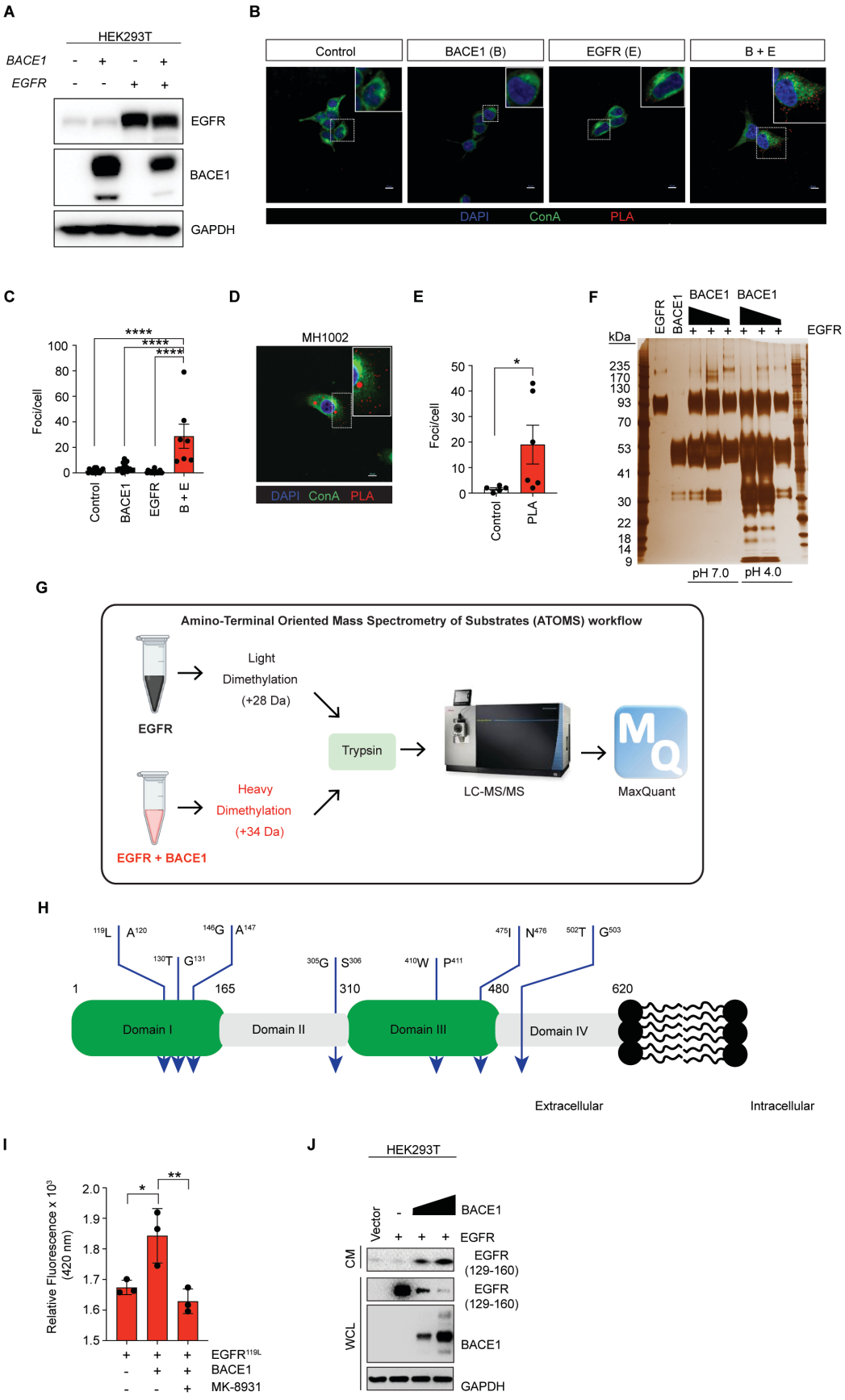
A
HEK293T
BACE1 - + - +
EGFR - - + +
EGFR
BACE1
GAPDH
B
Control
BACE1 (B)
EGFR (E)
B + E
DAPI ConA PLA
C
Foci/cell
Control
BACE1
EGFR
B + E
D
MH1002
DAPI ConA PLA
E
Foci/cell
Control
PLA
F
EGFR
BACE1
BACE1 BACE1
EGFR
kDa
pH 7.0
pH 4.0
G
Amino-Terminal Oriented Mass Spectrometry of Substrates (ATOMS) workflow
EGFR
Light Dimethylation (+28 Da)
Heavy Dimethylation (+34 Da)
EGFR + BACE1
Trypsin
LC-MS/MS
MaxQuant
H
Domain I
Domain II
Domain III
Domain IV
Extracellular
Intracellular
I
Relative Fluorescence x 10³ (420 nm)
EGFR119L
BACE1
MK-8931
J
HEK293T
Vector
BACE1
EGFR
CM
WCL
EGFR (129-160)
EGFR (129-160)
BACE1
GAPDH

Fig. 7. EGFR is a novel substrate of BACE1. (**A**) Western blot analysis of the indicated lysates for BACE1, EGFR (1150-C) and GAPDH following 72 hour expression of the indicated plasmids in HEK293T cells (*N*=2). (**B**) Micrographs depicting proximity-dependent amplification of signal following staining in HEK293T cells expressing *EGFR* and *BACE1* for 72 hours for EGFR and BACE1 (*N*=2). Scale bar = 10 μm. (**C**) Quantification of PLA foci per cell from images in (B). (**D**) Micrographs depicting BACE1 and EGFR PLA signal in MH1002 cells (*N*=2). Scale bar = 10 μm. (**E**) Quantification of PLA foci per cell from images in (D). (**F**) Silver stain analysis following co-incubation of rBACE1 and rEGFR overnight at 37 ºC. 0.25 µg of rEGFR was incubated with 0.5, 2 or 4 µg of rBACE1 in 0.1 M sodium acetate buffer pH 4.0 or 7.0 (*N*=2). (**G**) Schematic of the ATOMS workflow. (**H**) Domain schematic of the ectodomain of EGFR (domains I-IV) highlighting ATOMS identified cleavage sites (blue arrows) following 24 hour co-incubation of rBACE1 and rEGFR (ectodomain) at 37 °C. (**I**) BACE1 FRET activity assay measuring cleavage of EGFR peptide encompassing the ^{119}L↓A^{120} cleavage site following co-incubation in the presence or absence of MK-8931 (1 μM) for 24 hours at 37 °C (*N*=2). (**J**) Western blot analysis of the indicated proteins in conditioned media (CM) or whole cell lysates (WCL) from cells transiently expressing the indicated genes for 72 hours (*N*=2). EGFR (129-160) recognizes an epitope near the N-terminus of EGFR between amino acids 129 and 160. Bars in (C) and (E) indicate mean ± SEM. Bars in (I) indicate mean ± SD. Data in (C) and (I) were analyzed by one-way ANOVA followed by Tukey's multiple comparisons test. Data in (E) were analyzed by Mann-Whitney U test. **P*<0.05, ***P*<0.01, *****P*<0.0001.

Supplementary Materials for

Genome-wide *in vivo* CRISPR activation screen identifies BACE1 as a therapeutic vulnerability of lung cancer brain metastasis

Shawn C. Chafe, Kui Zhai, Nikoo Aghaei, Petar Miletic, Zhi Huang, Kevin R. Brown, Daniel Mobilio, Daniel Young, Yujin Suk, Shan Grewal, Dillon McKenna, Zahra Alizada, Agata M. Kieliszek, Fred C. Lam, Laura Escudero, Qian Huang, Ariana Huebner, Jack Lu, Patrick Ang, Alisha Anand, Stefan Custers, Erika Apel, Sarah Slassi, Benjamin Brakel, Jongmyung Kim, James K. C. Liu, Blessing Iquo Bassey-Archibong, Rober Abdo, Yaron Shargall, Jian-Qiang Lu, Jean-Claude Cutz, Qi Zhang, Shawn Shun-Cheng Li, Chitra Venugopal, Robert E. Hynds, Antoine Dufour, Jason Moffat, Charles Swanton, Shideng Bao, Sheila K. Singh

Corresponding author: Sheila K. Singh ssingh@mcmaster.ca; Shideng Bao baos@ccf.org

The PDF file includes:

- Materials and Methods
- Figs. S1 to S6
- Tables S1 and S6

Other Supplementary Materials for this manuscript include the following:

- Movies S1 and S2

Materials and Methods

Cell lines

The human lung cancer cell lines, A549 (RRID: CVCL_A549) and H1573 (RRID: CVCL_1478), were obtained from the American Type Culture Collection (ATCC). The H1299 (RRID: CVCL_0060) human lung cancer cell lines were kindly gifted by Dr. Andrei Ivanov from the Lerner Research Institute at Cleveland Clinic. The PC9 (RRID: CVCL_B260) and H1975 (RRID: CVCL_1511) cells were generous gifts from Dr. Don Nguyen from the Yale School of Medicine. The MH1002, MH1012, BT530, BT478 and MBT456 patient-derived cell lines were generated in our own laboratories from metastatic brain specimens of lung adenocarcinoma origin. The primary lung adenocarcinoma lines, CRUK0748-XCL and CRUK0733-XCL, were derived from subcutaneous patient-derived xenograft models established within the TRACERx study following serial implantation in NSG mice (*13*). All lung cancer cell lines were maintained in Neurobasal medium (Invitrogen, 12349015) supplemented with B-27 (Invitrogen, 12587010), 2 mM glutamine (ThermoFisher, 35050061), non-essential amino acids (ThermoFisher, 11140050), 1 mM sodium pyruvate (ThermoFisher, 11360070), 20 ng/mL epidermal growth factor (EGF, Goldbio, 1150-04-100), and 20 ng/mL basic fibroblast growth factor (bFGF, R&D Systems, 4114-TC-01M). The 293FT cells (Clontech; 632180, RRID: CVCL_6911) were maintained in the DMEM medium supplemented with 10% FBS. All cells used in this study were consistently confirmed to be free from mycoplasma by using a MycoFluor™ Mycoplasma Detection Kit (ThermoFisher, M7006). Unless otherwise indicated, media

was supplemented with antibiotic-antimycotic solution (ThermoFisher, 15240062) to prevent contamination.

Chemicals and Reagents

MK-8931 was purchased from Selleckchem (S8173) or Medkoo (331024). AZD3293 (S8193) and AZD3839 (S7731) were purchased from Selleckchem and PF-06751979 (555239) was purchased from Medkoo. Osimertinib was purchased from Selleckchem (S7297). D-Luciferin was purchased from GoldBio (LUCK-10G) and Perkin Elmer (122799). 32% Paraformaldehyde (PFA, 15714) was from Electron Microscopy Sciences and diluted to 4% with PBS before use. Protease (04693159001) and phosphatase inhibitor (04906837001) tablets were from Roche. All other chemicals and reagents were purchased from Sigma-Aldrich.

Human Surgical Specimens

The human surgical specimens of human lung cancer brain metastases were collected from the Brain Tumor and Neuro-Oncology Center at Cleveland Clinic according to a protocol approved by the Cleveland Clinic Institutional Review Broad as well as from the Hamilton General Hospital and St. Joseph's Healthcare Hamilton according to a protocol approved by the Hamilton Integrated Research Ethics Board (HiREB #4917). The surgical specimens were used for isolation of lung cancer cells, immunohistochemical or immunofluorescent analyses. The tissue microarray of primary lung cancer (LC1923) was from US Biomax Inc. The tissue microarray of 21 matched primary lung cancer lung tumors and their corresponding metastatic brain tumors was previously described (*30*). The fidelity of all patient samples was confirmed by a pathologist (J.,-Q.,L; J.,-C.,C, Q.Z)

Plasmids

The human *BACE1* sgRNA CRISPR/Cas9 All-in-One Lentivectors (K0166207 and K0166208) and the scrambled sgRNA CRISPR/Cas9 All-in-One Lentivector (K010) were purchased from ABM. The vectors for expressing human EGFR ORF (EX-A8661-Lv158) or BACE1 ORF (EX-U0498-Lv128) were purchased from GeneCopoeia. The dCas9-VP64-BLAST (pXPR_109)(Addgene #61425, RRID: Addgene_61425) and the $EGFR^{L858R}$ (pHAGE-$EGFR^{L858R}$)(Addgene #116276, RRID: Addgene_116276) plasmids were purchased from Addgene. The lentiviral GFP-luciferase plasmid was a kind gift from Fred C. Lam.

Library preparation

Human Calabrese CRISPR activation pooled library set A was a gift from David Root and John Doench (Addgene #92379). This pooled plasmid library was used to produce lentivirus as previously described (*16*). Briefly, twenty 80% confluent 150 mm dishes of HEK293T cells (~12 million cells per plate) were transfected with pCMV-VSVG (4.2 μg) (Addgene #8454, RRID: Addgene_8454), psPAX2 (42 μg) (Addgene #12260, RRID: Addgene_12260), library plasmid pool (33.3 μg) (Addgene #92379, RRID: Addgene_92379), and XtremeGENE™ 9 (238.5 μL) (Roche), and mixed in a total of 2 mL OptiMEM (ThermoFisher) and added to each plate of HEK293T cells containing (D10V) DMEM containing 10% FBS, 1x NEAA, 1 mM HEPES and 1 mM sodium butyrate (Sigma #B5887). Media was harvested and exchanged with fresh media on days 2-4. On day five, viral particles were pelleted via ultracentrifugation at 20,000 rpm for two hours at 4°C, and concentrated virus was stored at 4°C overnight, followed by long-term storage at -80°C.

Generation of CRISPR activation cell lines

CRUK0733-XCL and CRUK0748-XCL cell lines were transduced with lentivirus encoding dCas9-VP64 (D). Transduced cells were selected with blasticidin. Once expanded, CRUK0733-XCL-D and CRUK0748-XCL-D cells were transduced with lentivirus encoding GFP-luciferase (GL). Transduced cells were selected by flow cytometry and sorted by FACS. CRUK0733-XCL-GLD and CRUK0748-XCL-GLD cells were used in CRISPR activation studies.

CRISPRa Screen

To achieve 500X representation of the Calabrese library A, we deduced that we needed a final cell population of $5x10^7$ cells infected with the library to be injected into the lungs of 30 mice ($2x10^6$ cells per mouse lung). CRUK0748-XCL-GLD cells were transduced with Calabrese Library A lentivirus at an MOI of ~0.3 overnight and then selected with puromycin for 72 hours. Following selection, plates were split and cells allowed to grow for 48 hours in media free of puromycin to recover prior to inoculation of mice. At this point, $3x10^7$ cells were harvested for a T_0 cell pellet (initial screen timepoint) and frozen at -80°C to be sequenced at a later stage, and $6x10^7$ cells were prepared for inoculation of mice. The cell suspension was then prepared to deliver $2x10^6$ cells per mouse in a final volume of 70 μL in PBS containing 10% Matrigel™ (Corning). In parallel, CRUK0748-XCL-GLD cells from control plates exposed to neither Calabrese A virus nor puromycin were dissociated and prepared for control injections (*n*=4). Library-transduced cells were then injected into 30 NSG mice, representing greater than 500x coverage of the library, via the modified thoracotomy orthotopic intrathoracic injection (*below*). Tumor burden was monitored weekly by bioluminescent imaging (BLI) until mice became moribund (Day 26-

29) at which time mice were injected with 150 mg/kg d-luciferin, lungs and brains removed and brains imaged by BLI and then flash frozen until genomic DNA could be extracted.

Genomic DNA extraction and sequencing

Genomic DNA was extracted from lung and brain tissue using the Gentra Puregene Tissue kit from Qiagen (#158689). Isolated DNA was phenol:chloroform extracted and ethanol precipitated to improve DNA quality before proceeding. sgRNAs were amplified using previously described primers (and listed here in Table S6) and reaction conditions (*16*) using PrimeStar GXL DNA polymerase (TakaraBio, R050A). 12 brain samples and 11 lung samples were sequenced on a NovaSeq SP flow cell with a paired-end 100 bp kit with 10-15% PhiX DNA spike in performed by The Centre for Applied Genomics, The Hospital for Sick Children, Toronto, Canada. Each sample received 30-40M reads and indexed reads were demultiplexed prior to analysis.

Data Analysis

Reads underwent quality assurance, end-trimming (cutadapt and trim galore) using the Galaxy toolshed (*44*). Reads were then aligned to the Calabrese Library A index file using Bowtie v1.3.1 allowing for single nucleotide mismatches and discarding reads that aligned to more than a single sgRNA. Aligned reads for each sample were then assembled into a read matrix file and analyzed using R. sgRNA read counts were normalized to one million reads per sample and were then averaged across all lungs and brains to determine the mean normalized read count per sgRNA. The mean read counts per sgRNA were then averaged for the top 2 abundant sgRNAs targeting each gene to determine the mean normalized sgRNA read count per gene. This was determined for both lungs and brains. The mean normalized read count per gene was utilized when determining the fold change

(FC) in normalized sgRNA read counts per tissue per animal relative to control sgRNAs and plotted as rug plots. FC = (normalized read count targeting sgRNA/mean normalized read count control sgRNA). The normalized read counts per gene were also expressed as fold change relative to the control sgRNAs in their respective tissue. This was determined for both lungs and brains to determine the relative increase in abundance of each sgRNA in the brains relative to the lungs and plotted as violin plots.

Lentivirus production and *BACE1* knockout cell generation

Lentiviruses were produced in 293FT cells and prepared as previously described (*28*). Briefly, 293FT cells were co-transduced with targeting plasmids and packaging vectors pCMV-VSVG and psPAX2 by using PEI (Serochem, AQ100). Four days after transfection, the supernatants were harvested and virus titers were determined as described previously (*28*). For infection, cells were treated with lentivirus at a multiplicity of infection (MOI) of 1. CRISPR/Cas9 was used to generate *BACE1* KO lung cancer cells. Briefly, MH1002 or H1299 cells were infected by lentiviruses expressing human *BACE1* sgRNA CRISPR/Cas9 All-in-One Lentivectors or the scrambled sgRNA CRISPR/Cas9 All-in-One Lentivector (K010) for 12 hours. Two days after infection, the cells were treated with 2 μg/mL puromycin (Fisher Scientific, BP2956100) for seven days. After treatment, single-cell clones were cultured. Western blot analysis confirmed successful knockout of *BACE1*.

PDX Establishment and Drug Treatment *in vivo*

All animal experiments were performed in accordance with protocols approved by the IACUC of the Lerner Research Institute at the Cleveland Clinic (AUP# 2559) and the AREB (AUP# 22-12-38) of McMaster University. Six- to eight-week old NSG mice

(NOD.Cg-*Prkdc*^{scid}*Il2rg*^{tm1Wjl}/SzJ) were used for establishing PDXs derived from human lung cancer cells for the *in vivo* studies. Mice were maintained in a 12-hour light/12-hour dark cycle, and provided with sterilized water and food *ad libitum* at the Biological Resource Unit of the Cleveland Clinic Lerner Research Institute or the Central Animal Facility (CAF) of McMaster University.

To establish xenografts for *in vivo* studies, transplantation of WT or *BACE1* KO MH1002 cells into the brains of NSG mice was performed as described previously (*17*). *In vivo* bioluminescent imaging was performed twice per week to monitor tumor growth, using the Spectrum CT Imaging System (PerkinElmer), before and after treatment. For drug treatment, a stock solution of MK-8931 at 100 mg/mL in DMSO was diluted in 0.5% (w/v) methylcellulose (Sigma-Aldrich, M0512) to 6 mg/mL (*31*). Mice bearing xenografts from WT MH1002 cells or CRISPR activated-*BACE1* CRUK0748-XCL-GLD cells were treated with MK-8931 (30 mg/kg) or the control (DMSO) once daily by oral gavage for three weeks or until humane endpoint was reached. To collect mouse brains bearing tumors, cardiac perfusion with PBS and 4% PFA was performed. The brains were fixed and sectioned for further immunofluorescent, histochemical and histological analyses.

Thoracotomy model

Mice are anesthetized with isoflurane and provided with pre-operative buprenorphine (0.5 mg/kg), carprofen (5 mg/kg) and saline. Mice are then immobilized with the right forelimb immobilized above the head to expose the right chest. Fur is removed over the surgical site with scissors and the surgical site cleaned with 7% followed by 10% iodine scrub. A 1 cm incision is made in the skin over the rib cage to visualize the lungs. A superficial injection of the cell suspension ($5x10^5$ cells) in 10% Matrigel™ is made between the ribs

directly into the lung. The wound is sutured and glued closed with tissue glue and the mice allowed to recover on heatpads in fresh cages. Metastatic growth was determined by *ex vivo* BLI of brains, livers and leg bones and visualized with petal plots using the ggplot2 function in R. Petal height indicates average total bioluminescent flux (0-10^8) for the group for that organ. Petal width (0-1) depicts the metastatic penetrance for the group. *n*=8 per group.

Intracardiac model

Mice are anesthetized with isoflurane. Mice are then immobilized in the supine position with forelimbs immobilized overhead. The chest is sterilized with 70% ethanol and an injection made 3 mm to the left of midline in line with the left axilla. $2x10^5$ cells in sterile saline are slowly administered with a 0.5 cc insulin syringe (29G x ½") in 50 μL. Mice are allowed to recover on heatpads in fresh cages.

Sphere Formation Assay

Ten thousand lung cancer cells were plated per well of a 12-well plate and maintained in stem cell medium. For studies involving drug treatment, MK-8931 (30 μM) or DMSO was added to cells and incubated for four days. After seven days, tumor-spheres were imaged by EVOS FL microscope (AMG). The sizes and numbers of spheres in the control and MK-8931 groups were further analyzed with ImageJ.

Cell Viability Assay

Cell viability assay was performed by using a Cell Titer-Glo Luminescent Cell Viability Assay Kit according to the manufacturer's instruction (Promega, G7571). For this assay, 1,000 cells were seeded per well of a 96-well plate in 100 μL of stem cell medium. Then, MK-8931, Osimertinib or DMSO (control) was added to cells. At indicated days, 50 μL of

the Cell-Titer Glo reagent was added to each well and incubated for 15 minutes. Luminescence was measured using the VICTOR Multilabel Plate Reader (PerkinElmer). For synergy experiments, cells were treated with the indicated concentrations of MK-8931 and Osimertinib for 72 hours. Viability data was input into SynergyFinder 3.0 (*45*) to determine whether the two drugs were synergistic (score greater than 10), additive (score between -10 and 10) or antagonistic (less than -10). Scores were calculated using the BLISS synergy model.

Spheroid invasion assay

2000 cells were seeded per well in ultra-low attachment U-bottom 96 well plates in 100 μL NCC, spun for 10 minutes at 1200 rpm and allowed to form spheres for 72 hours. Plates were placed in an Incucyte® and imaged every eight hours over the course of the 72 hours to confirm sphere formation. Following the 72 hour incubation, Matrigel™ was added in 100 μL to achieve a final concentration of 17.5% (CRUK0733-XCL-GLD) or 50% (H1299$^{GFP\text{-}Luc}$), plates incubated at 37°C for 30 minutes and then placed in the Incucyte® for 10 days. Plates were imaged every eight hours for 10 days to track invasion of cells into the surrounding Matrigel™. Changes in sphere size and invasion area were calculated using the Incucyte® spheroid analysis software module or in ImageJ.

Transwell migration assay

CRUK0748-XCL cells (10^5 per insert) were seeded on polycarbonate inserts with 8.0 mm membrane pores in 24-well plates (Costar #3422) and maintained in DF12 medium for 48 hours. Cells were washed with cold PBS and those unmigrated cells (on the top of the insert) were completely removed gently using a cotton swab. The migrated cells (on the underside of the insert) were fixed with cold methanol and stained with crystal violet. After

washing away the dye, inserts were dried out and mounted on the glass slides. Images were captured with a Leica DMIRB microscope and the density of migrated cells was analyzed in ImageJ.

Immunofluorescence and immunohistochemistry

Immunofluorescent staining of tumor tissues or cells was performed as described previously (*28*). In brief, tumor sections or cells were fixed with 4% PFA for ten minutes, washed three times with cold PBS for five minutes each, permeabilized with 0.5 % (v/v) triton X-100 (Bio-Rad, 1610407) for ten minutes, and blocked with 3% (w/v) BSA (Sigma-Aldrich, A7906) in PBS for one hour at room temperature. Antigen retrieval was performed by incubating the sections in boiled antigen retrieval buffer (Vector Laboratories, H-3300) for 15 minutes. Primary antibodies were added to the sections or cells and incubated overnight at 4ºC. Primary antibodies used for immunofluorescence in this study were diluted as described below: anti-BACE1 (Abcam, ab2077, RRID: AB_302817, 1:50; Thermo Fisher Scientific, MA1-177, RRID: AB_2608440, 1:50) and anti-EGFR^{Y1068} (Abcam, ab40815, RRID: AB_732110, 1:100). After the incubation of the primary antibodies, the sections or cells were washed three times with cold PBS for five minutes each and then incubated with the secondary antibodies for one hour at room temperature. The secondary antibodies used in this study included Alexa Fluor® 488 Donkey Anti-Mouse IgG (Invitrogen, A-21202, RRID: AB_141607, 1:200), Alexa Fluor® 488 Donkey Anti-Rabbit IgG (Invitrogen, A-21206, RRID: AB_2535792, 1:200), Alexa Fluor® 488 Donkey Anti-Goat IgG (Invitrogen, A-11055, RRID: AB_2534102, 1:200), and Alexa Fluor® 488 Goat Anti-Rabbit (Invitrogen, A-11008, RRID: AB_143165, 1:200). For immunohistochemistry studies, HRP-conjugated secondary antibodies to rabbit (Abcam,

ab214880, RRID: AB_3106917) and mouse (Abcam, ab214879, RRID: AB_3678671) were utilized according to the manufacturer's instructions. After washing three times with cold PBS for five minutes each, the sections or cells were counterstained by DAPI (Cell Signaling, 4083, 1:5000) and sealed with mounting medium (Sigma-Aldrich, F4680). Finally, images were captured by a fluorescence microscope (Leica DM4000) and further analyzed with ImageJ software (https://imagej.nih.gov/). The scores of BACE1 expression were based on BACE1+ cells in the samples: < 25% = 0; 25% - 50% = 1+; 50% -75% = 2+; and > 75% = 3+. The landmark time for KM curves was discovery of the BM.

Flow Cytometry

1 x 10^6 CRUK0748-XCL-GLD cells expressing control or *PTPRC* targeting sgRNA were stained with anti-CD45 APC Cyanine 7 antibody (BioLegend, 368515, clone 2D1, RRID: AB_2566375, 1:50) for 20 minutes at room temperature in staining buffer (PBS, pH 7.4, containing 2 mM EDTA). Cells were washed with staining buffer and stained with 7AAD (BioLegend, 420403, 1:100). Viable cells were analyzed on a CytoFlex (Beckman Coulter) for CD45 expression.

Immunoblot

Immunoblot analysis was performed as previously described (*28*). Briefly, cells were lysed with RIPA buffer [50 mM TrisHCl (pH7.4), 150 mM NaCl, 2 mM EDTA, 1% (v/v) NP-40, 0.1% (w/v) SDS, protease inhibitor (one tablet per 10 mL of RIPA buffer, Roche) and phosphatase inhibitor (one tablet per 10 mL RIPA buffer, Roche) for 20 minutes on ice. Cell lysates or conditioned medium were collected and subjected to SDS-PAGE and blotted onto PVDF membranes (ASI, XR730). After blocking with 5% (w/v) non-fat milk

(RPI, M17200) in TBST, the membranes were incubated with primary antibodies overnight at 4°C. The following primary antibodies were used in this study anti-BACE1 (Santa Cruz, sc-33711, RRID: AB_626716, 1:500), anti-EGFR (Bethyl Laboratories, A300-388AM, RRID: AB_386099, 1:1000; Santa Cruz, sc-365829, RRID: AB_10844017, 1:500), anti-EGFR^{Y1068} (Cell Signaling, 2234, RRID: AB_331701, 1:1000), anti-ERK1/2 (BioLegend, 686902, RRID: AB_2629535, 1:1000), anti-ERK1/2$^{T202/Y204}$ (Cell Signaling, 9106, RRID: AB_331768, 1:1000), anti-cJun (Cell Signaling, 2315, RRID: AB_490780, 1:1000), anti-cJun^{S63} (Cell Signaling, 2361, RRID: AB_490908, 1:1000), anti-MEK1 (Cell Signaling, 2352, AB_10693788, 1:1000), anti-MEK1/2$^{S217/221}$ (Cell Signaling, 9154, RRID: AB_2138017, 1:1000), and anti-GAPDH (Cell Signaling, 2118, RRID: AB_561053, 1:3000). After incubation with primary antibodies, the membranes were washed three times with TBST for ten minutes each. Membranes were then incubated with HRP-linked secondary antibodies in 5% milk for one hour at room temperature. Species specific HRP-linked secondary antibodies used were anti-mouse IgG (Cell Signaling, 7076, RRID: AB_330924, 1:5000), anti-rabbit IgG (Cell Signaling, 7074, RRID: AB_2099233, 1:5000), and anti-goat IgG (Santa Cruz, sc-2354, RRID: AB_628490, 1:5000). After washing three times with TBST for ten minutes each, signals on the membranes were developed using enhanced chemiluminescence (Advansta, K-12045) and images were acquired by a molecular imager (Bio-Rad, Universal Hood II) and analyzed by the Image Lab software (Bio-Rad).

Phospho-kinase array

Lysates from BACE1^{KO} cells were incubated with membranes from the human Proteome Profiler™ phospho-kinase array kit (R&D Systems, ARY003B) according to the

manufacturer's instructions. Membranes were developed with enhanced chemiluminescence and imaged on a Chemi-Doc. Signal intensity for duplicate spots was calculated using ImageLab software and comparisons in intensity per condition made in Prism.

***In vitro* cleavage of EGFR**

Recombinant catalytic domain of BACE1 (rBACE1) was purchased from R&D Systems (931-AS-050). Recombinant ectodomain of EGFR (rEGFR) was purchased from Sino Biological (10001-H08H). The two proteins were incubated together in 0.1 M sodium acetate buffer, pH 4.0 or pH 7.0, overnight at 37 °C. 0.25 µg of rEGFR was combined with 0.5, 2 or 4 µg of rBACE1 corresponding to a molar ratio of 1:1, 5:1 or 10:1 rBACE1:rEGFR. Reactions were stopped by the addition of 4X LDS sample buffer (Thermofisher, NP0007). To resolve cleavage products, reactions were electrophoresed on a 4-12% bis-tris gradient gel alongside BLUeye prestained protein ladder (FroggaBio, PM007-0500) and then silver stained (Pierce Silver Stain kit, Thermofisher, 24612) according the manufacturer's recommendations.

Amino-terminal oriented mass spectrometry of substrates (ATOMS) analysis of EGFR cleavage by BACE1

ATOMS employs isotopic labeling and quantitative tandem mass spectrometry to identify proteolytic cleavage sites (*37*). Isotopic labeling was carried out as previously described (*37*). 2 µg of protein, either BACE1 digested EGFR (in a protease to substrate ratio of 16:1 for 24 h) or EGFR alone, were reduced using a final concentration of 25 mM dithiothreitol (DTT) (Gold Biotechnology, St- Louis, MO) in 200 mM HEPES at 37 °C for 1 h. Samples were then alkylated to a final concentration of 60 mM iodoacetamide (IAA)

(GE Healthcare, Mississauga, ON) for 20 minutes in the dark at room temperature, followed by a quenching reaction to a final concentration of 40 mM DTT for 25 minutes at room temperature. The generated N-termini and lysines were isotopically labeled: the BACE-1 and EGFR sample was isotopically labeled with a final concentration of 20 mM deuterated heavy formaldehyde (13CD2O) (Cambridge Isotope Laboratories, Tewsbury,MA) and EGFR without BACE-1 sample was labeled with a final concentration of 20 mM light formaldehyde (12CD2O) (VWR Chemicals, Mississauga, ON) with the addition of 40 mM sodium cyanoborohydride (Sigma-Aldrich, Oakville, ON). The pH was then adjusted to 6.5 and incubated at 37 °C overnight. All of the sample was loaded on a 10% polyacrylamide protein gel and ran for 30 minutes at 60 volts. The gel was then stained by addition of 50 mL of 0.1 % Coomassie Brilliant Blue (VWR m140-10g) in a 50% methanol, 10% acetic acid solution and incubated at room temp for 30 minutes on a rocker. The gel was then destained by 3 washes for 10 minutes each in a 50% methanol, 10% acetic acid solutions. The gel was then imaged and the band containing all of the proteins was extracted by razor blade and stored in distilled water overnight at 4 °C. The gel was minced into ~1 mm cubed slices. Excess Coomassie Brilliant Blue stain was removed by 3 washes in a 50% acetonitrile, 50 mM ammonium bicarbonate solution with gentle shaking for 15 minutes. The gel was then dehydrated with 3 washes of 100% acetonitrile washes for 15 minutes. The gel was then rehydrated in 20 μL of a 10% acetonitrile, 40 mM ammonium bicarbonate buffer containing 0.02 μg/μL trypsin (ThermoFisher, #90051) for 2 hours at 37 °C. Followed by an additional 30 μL of trypsin solution before an overnight digestion. Peptides were extracted from the gel by the addition of an extraction solution containing 60% acetonitrile, 1% Trifluoroacetic acid, the

gel was washed 3 times in extraction solution with gentle shaking at room temperature for 10 minutes. After each incubation the solutions were collected and pooled into a fresh low protein binding tube. The extraction solution was removed by lyophilization in a Savant RT 100 speed vac. The peptides were resuspended in 0.1% Trifluoroacetic acid with gentle shaking for 30 minutes at room temperature. The sample was then subjected to c18 clean up by Sep-Pak solid phase extraction cartridges (Waters Mississauga, ON). Sep-Pak columns were conditioned with 1 x 3mL 90% methanol/0.1% TFA, washed with TFA, 1 x 2mL 0.1% TFA acid. Each sample was loaded onto a column and washed with 1x 3mL 0.1% TFA/5% methanol. Peptides were eluted from the column with 1 x 1mL 50% ACN/0.1% formic acid and lyophilized and submitted for liquid chromatography (LC)-tandem mass spectrometry (MS/MS) analysis to the Southern Alberta Mass Spectrometry core facility, University of Calgary, Canada. The LC-MS/MS data are analyzed using the database search MaxQuant software package v.2.5.2.0 at a peptide-spectrum match false discovery rate (FDR) of <0.05. Experimental spectra were compared to a Targeted FASTA reference containing only the EGFR and BACE1 sequences obtained from Uniprot. Search parameter was specified for dimethylation of the N-termini and lysines as a label. This key feature ensures fully tryptic peptides, which canonically lack a dimethylated N-terminus are ignored by the search engine, leading to data enriched for protease generated peptides labeled both at their N-terminus and lysines if present.

BACE1 *in vitro* FRET activity assay

Recombinant BACE1 was incubated with amyloid precursor protein peptide with the Swedish mutation in the BACE1 cleavage site or with EGFR peptide labelled with FRET donor:acceptor pairs methyl coumarin (MCA) and dinitrophenol (Dnp). APP –

[(MCA)SEVNLDAEFRK(Dnp)RR] was purchased from R&D Systems (ES004). EGFR peptide containing the L119 BACE1 cleavage site [(MCA)NSYALAVLSN(Lys(Dnp))RR] corresponding to amino acids 115-124 of EGFR, EGFR peptide containing the T130 BACE1 cleavage site [(MCA)DANKTGLKEL(Lys(Dnp))RR], and the EGFR peptide contraining the G146 cleavage site [(MCA)EILHGAVRFS(Lys(Dnp))RR] all with two terminal arginines added to improve solubility, were purchased from GenScript. 0.1 μM BACE1 was incubated with 1 μM peptide for 30 minutes or 24 hours at 37 °C in 0.1 M sodium acetate buffer, pH 4.0. Liberation of fluorescence at 420 nm was measured in a Biotek Neo (Agilent) every 60 seconds for 30 minutes and then again after 24 hours. Parallel reactions were run in the presence of 1 μM MK-8931 to confirm any liberation of fluorescence was due to BACE1 activity.

$A\beta_{1-42}$ ELISA

Conditioned media was recovered from CRUK0748-XCL-GLD WT and BACE1-activated (Act #1 and Act#2) cells. Media was spun at 300 x g for 10 minutes to remove cellular debris. $A\beta_{1-42}$ levels were measured using the Human Amyloid beta (aa1-42) Quantikine ELISA kit (R&D Systems, DAB142) according to manufacturer's instructions. Briefly, conditioned media was diluted 1:1 with dilution buffer prior to assaying $A\beta_{1-42}$ levels. Absorbance levels were measured in a FLUOstar Omega (BMG Labtech) UV/vis spectrophotometer and $A\beta_{1-42}$ concentrations determined from interpolating from the standard curve.

Proximity ligation assays

MH1002 and HEK293T cells were seeded onto poly-L-ornithine and laminin coated coverslips or directly onto plastic coverslips, respectively. Cells were fixed,

permeabilized, blocked and incubated with primary antibodies against BACE1 and EGFR overnight as described in the immunofluorescence section above. Coverslips were washed and subjected to proximity ligation assay using the Duolink® In Situ Red Mouse/Rabbit kit (Sigma, DUO92101) as described by the manufacturer. Cells were mounted in aqueous mounting media containing DAPI and imaged on a Nikon A1R inverted confocal microscope equipped with a Hamamatsu Orca Flash 4.0 V3 sCMOS with 82% High Quantum Efficiency at the Centre for Advanced Light Microscopy (McMaster University). Quantitative analysis of PLA foci per cell was performed using ImageJ (v2.1.0). A Difference of Gaussians approach was applied using a Sigma value of 4 to reduce background noise (*46*). Binary 16-bit PLA images were then created using a minimum intensity threshold of 20 and foci were counted automatically (size set to 0.03-infinity, roundness set to 0.50-1.00). Nuclei were counted manually. Images of foci were enhanced with minimum and maximum display values of 27-188 for MH1002 samples, and 1-130 for HEK293 samples. For MH1002 samples, DAPI and ConA images were additionally enhanced with display values of 1-60 and 30-270, respectively.

BACE1 expression in the TRACERx 421 cohort

RSEM (v.1.3.3) (*47*) was used with default parameters to quantify gene expression on the full cohort of TRACERx 421 RNA-seq samples (*48*). Subsequently, only samples from lung adenocarcinoma tumors were considered. Expression of BACE1 was summarized across all available samples of a given tumor to calculate a median TPM (transcripts per million) per tumor. Lung adenocarcinoma tumors were split into those with a clonal EGFR driver mutation, those with a clonal KRAS driver mutation, and those with neither based

on the driver annotation described previously (*49*). In brief, mutations in KRAS or EGFR were classified as driver mutations, if there were ≥3 exact matches of the specific variant in the COSMIC cancer gene census (v.75) (*50*).

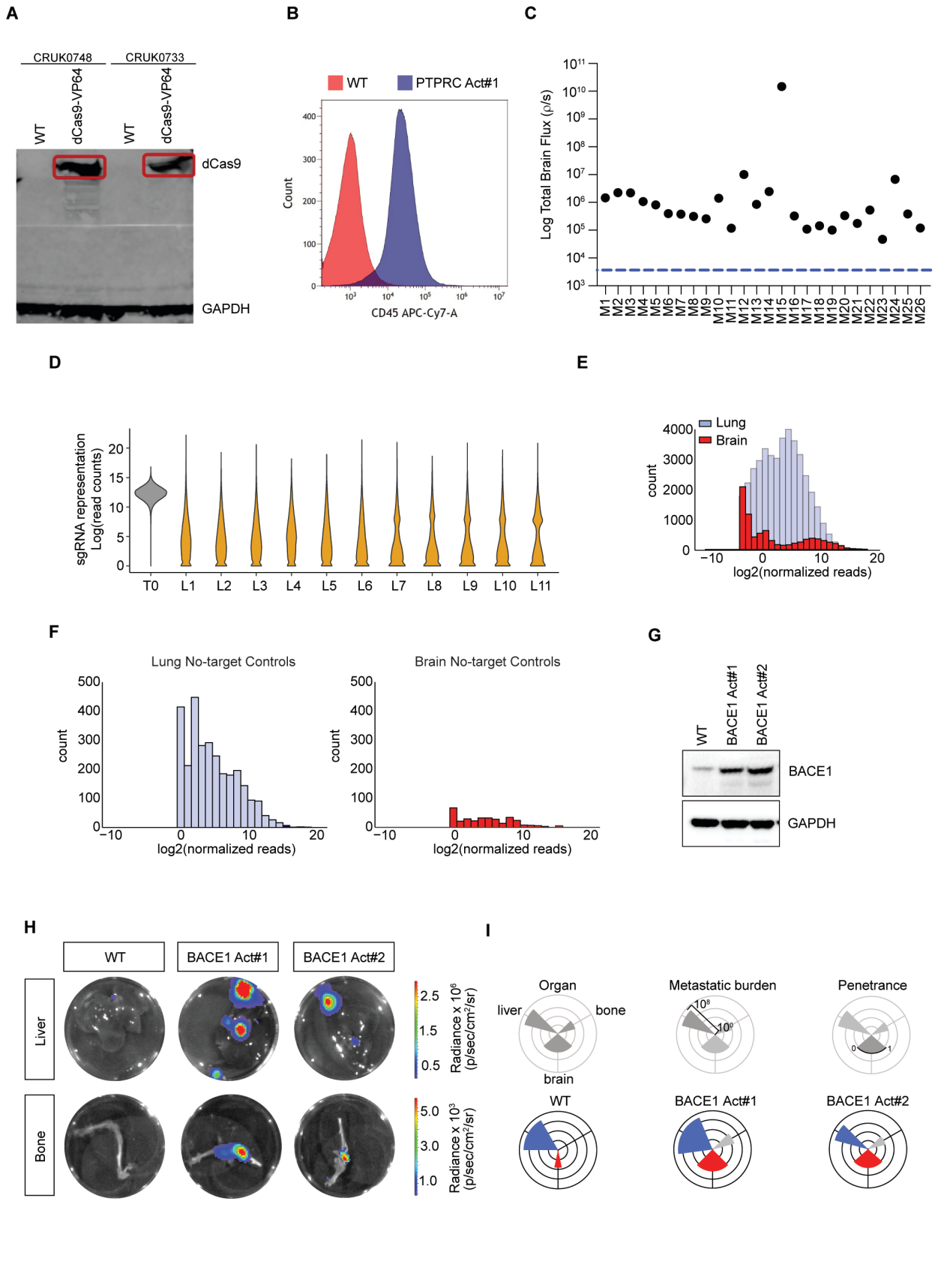
A
CRUK0748
CRUK0733
WT
dCas9-VP64
WT
dCas9-VP64
dCas9
GAPDH
B
WT
PTPRC Act#1
Count
CD45 APC-Cy7-A
C
Log Total Brain Flux (p/s)
D
sgRNA representation
Log(read counts)
T0
L1
L2
L3
L4
L5
L6
L7
L8
L9
L10
L11
E
Lung
Brain
count
log2(normalized reads)
F
Lung No-target Controls
Brain No-target Controls
count
log2(normalized reads)
G
WT
BACE1 Act#1
BACE1 Act#2
BACE1
GAPDH
H
WT
BACE1 Act#1
BACE1 Act#2
Liver
Bone
Radiance x 10^6 (p/sec/cm²/sr)
Radiance x 10^3 (p/sec/cm²/sr)
I
Organ
liver
bone
brain
Metastatic burden
Penetrance
WT
BACE1 Act#1
BACE1 Act#2

Fig. S1. *In vivo* CRISPR activation screen identifies *BACE1* drives LUAD brain metastasis. (**A**) Western blot analysis of dCas9 and GAPDH expression in the indicated cell lines. CRUK0748 – CRUK0748-XCL cells; CRUK0733 – CRUK0733-XCL cells. (**B**) Flow cytometry analysis for activation of CD45 expression in CRUK0748-XCL-GLD (WT) or CRUK0748-XCL-GLD cells transduced with sgRNA targeting *PTPRC* (PTPRC Act#1). (**C**) Bioluminescence values following *ex vivo* imaging of the brains of the mice in the screen at endpoint. Blue line – baseline bioluminescent signal from the brains of naïve mice. (**D**) Violin plot of the sgRNA representation across each of the lungs (L1-L11) analyzed from the screen relative to the T_0 cell inoculum sample. (**E**) Lung (blue) and brain (red) sgRNA distribution plots. (**F**) Distribution plots of the control sgRNAs in the lung (left) and brain (right). (**G**) Western blot analysis of BACE1 expression in the indicated CRUK0748-XCL-GLD cell lines following expression of *BACE1*-activating sgRNAs. GAPDH was used as a loading control. (**H**) Representative images of livers (top row) or bones (bottom row) from mice bearing orthotopic tumors from CRUK0748-XCL-GLD (WT) or BACE1-activated (BACE1 Act#1, Act#2) cells. Heat maps depict radiance levels for each organ. (**I**) Petal plots summarizing the metastatic tropism of the CRUK0748-XCL-GLD (WT) or BACE1-activated (BACE1 Act#1, Act#2) cell lines implanted orthotopically in (F). Petal height indicates average total bioluminescent flux ($0\text{-}10^8$) for the group for that organ. Petal width (0-1) depicts the metastatic penetrance for the group (*n*=8 per group, *N*=2).

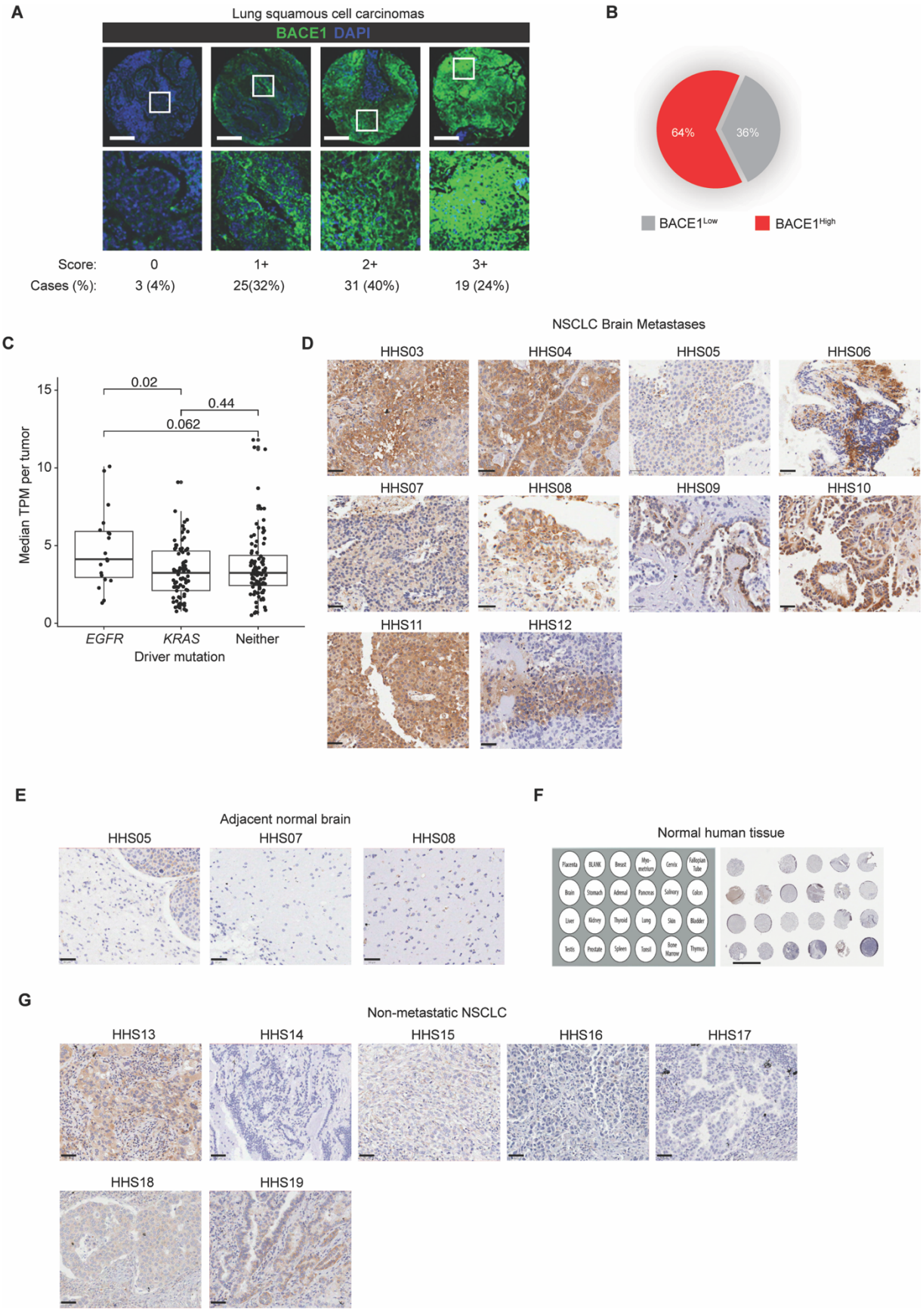
A
Lung squamous cell carcinomas
BACE1 DAPI
Score: 0 1+ 2+ 3+
Cases (%): 3 (4%) 25(32%) 31 (40%) 19 (24%)
B
64%
36%
BACE1Low
BACE1High
C
0.02
0.44
0.062
Median TPM per tumor
EGFR
KRAS
Neither
Driver mutation
D
NSCLC Brain Metastases
HHS03
HHS04
HHS05
HHS06
HHS07
HHS08
HHS09
HHS10
HHS11
HHS12
E
Adjacent normal brain
HHS05
HHS07
HHS08
F
Normal human tissue
G
Non-metastatic NSCLC
HHS13
HHS14
HHS15
HHS16
HHS17
HHS18
HHS19

1396

Fig. S2. BACE1 is expressed in LUAD brain metastasis and is associated with worse prognosis. (**A**) Immunofluorescent staining of BACE1 (green) in squamous cell lung carcinomas in a primary NSCLC TMA. Nuclei are counterstained with DAPI (Blue). Scale bar = 250 μm. (**B**) Pie chart depicting the frequency of tumor cores according to BACE1 expression. (**C**) Normalized BACE1 expression in the LUAD cases of the TRACERx 421 cohort associated with *EGFR* or *KRAS* clonal mutations. (**D**) Immunohistochemical staining of BACE1 in NSCLC brain metastases from Hamilton Health Sciences. Scale bar = 50 μm. (**E**) Immunohistochemical staining of BACE1 in adjacent normal brain regions from the indicated patients with NSCLC brain metastases. Scale bar = 50 μm. (**F**) Immunohistochemical staining of BACE1 in a normal human tissue microarray. Scale bar = 3 mm. (**G**) Immunohistochemical staining of BACE1 in non-metastatic human NSCLC tumors. Scale bar = 50 μm.

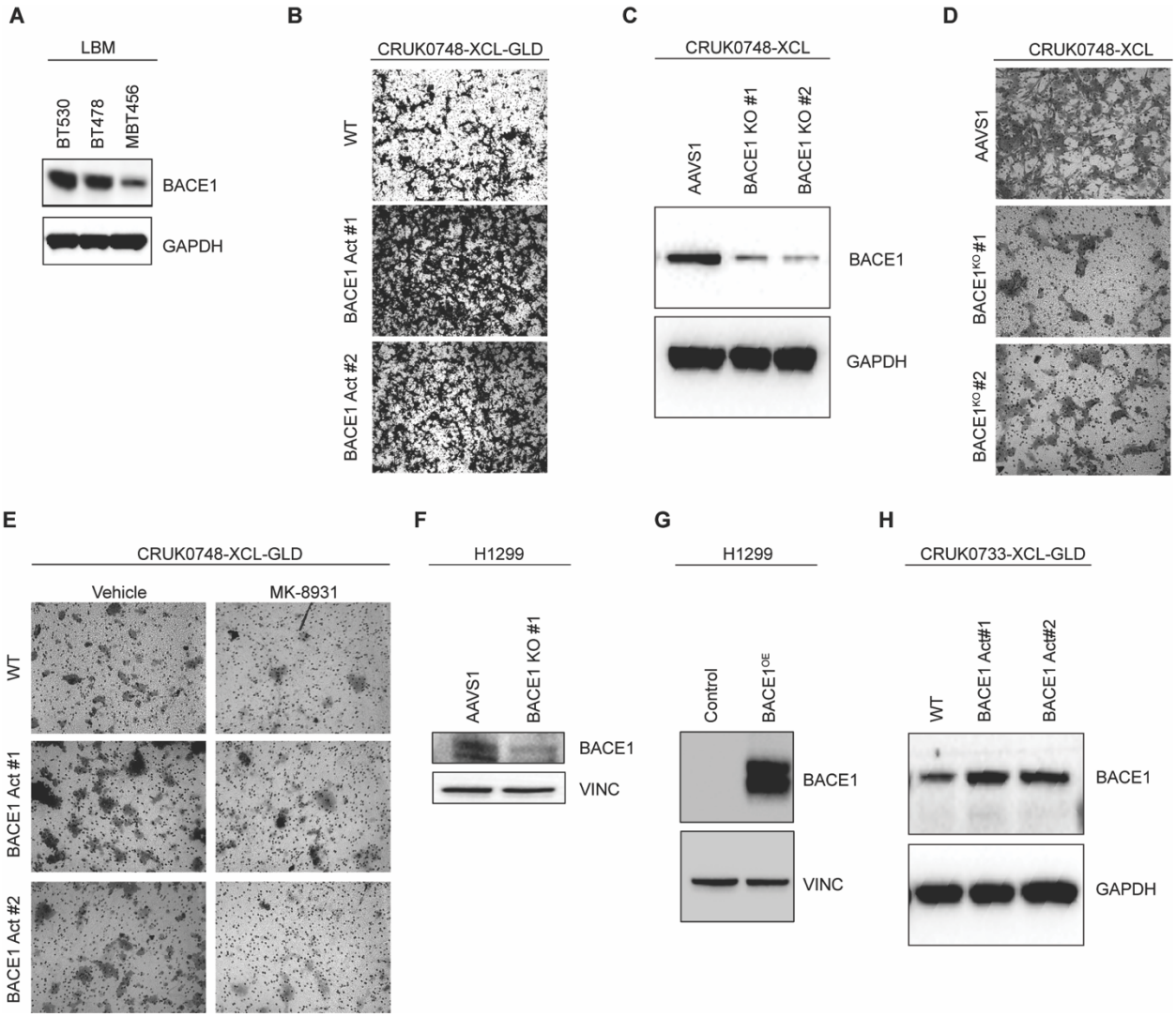

Fig. S3. BACE1 increases the migratory and invasive capacity of primary LUAD cells. (**A**) Western blot analysis of BACE1 expression in a panel of lung cancer brain metastasis initiating cells (*N*=2). (**B**) Representative micrographs of crystal violet stained cells depicting transwell migration of CRUK0748-XCL-GLD cells following BACE1 activation. Migration proceeded for 48 hours after the cells were seeded (*n*=6, *N*=3). (**C**) Western blot analysis of the indicated lysates from CRUK0748-XCL BACE1^{KO} cells for BACE1 and GAPDH expression. (**D**) Representative micrographs of crystal violet stained cells depicting transwell migration of *BACE1*^{KO} CRUK0748-XCL cells. Migration proceeded for 48 hours after the cells were seeded (*n*=4, *N*=3). (**E**) Representative micrographs of crystal violet stained cells depicting transwell migration of MK-8931 (10 μM) treated CRUK0748-XCL-GLD cells. Migration proceeded for 48 hours after the cells were seeded (*n*=6, *N*=3). (**F**) Western blot analysis of H1299$^{GFP\text{-}Luc}$ BACE1^{KO} cells for BACE1 and Vinculin expression (*N*=2). (**G**) Western blot analysis of H1299$^{GFP\text{-}Luc}$ cells over-expressing BACE1 for BACE1 and Vinculin expression (*N*=2). (**H**) Western blot

analysis of the indicated lysates from CRUK0733-XCL-GLD cells for BACE1 and GAPDH expression following activation of BACE1 (*N*=2).

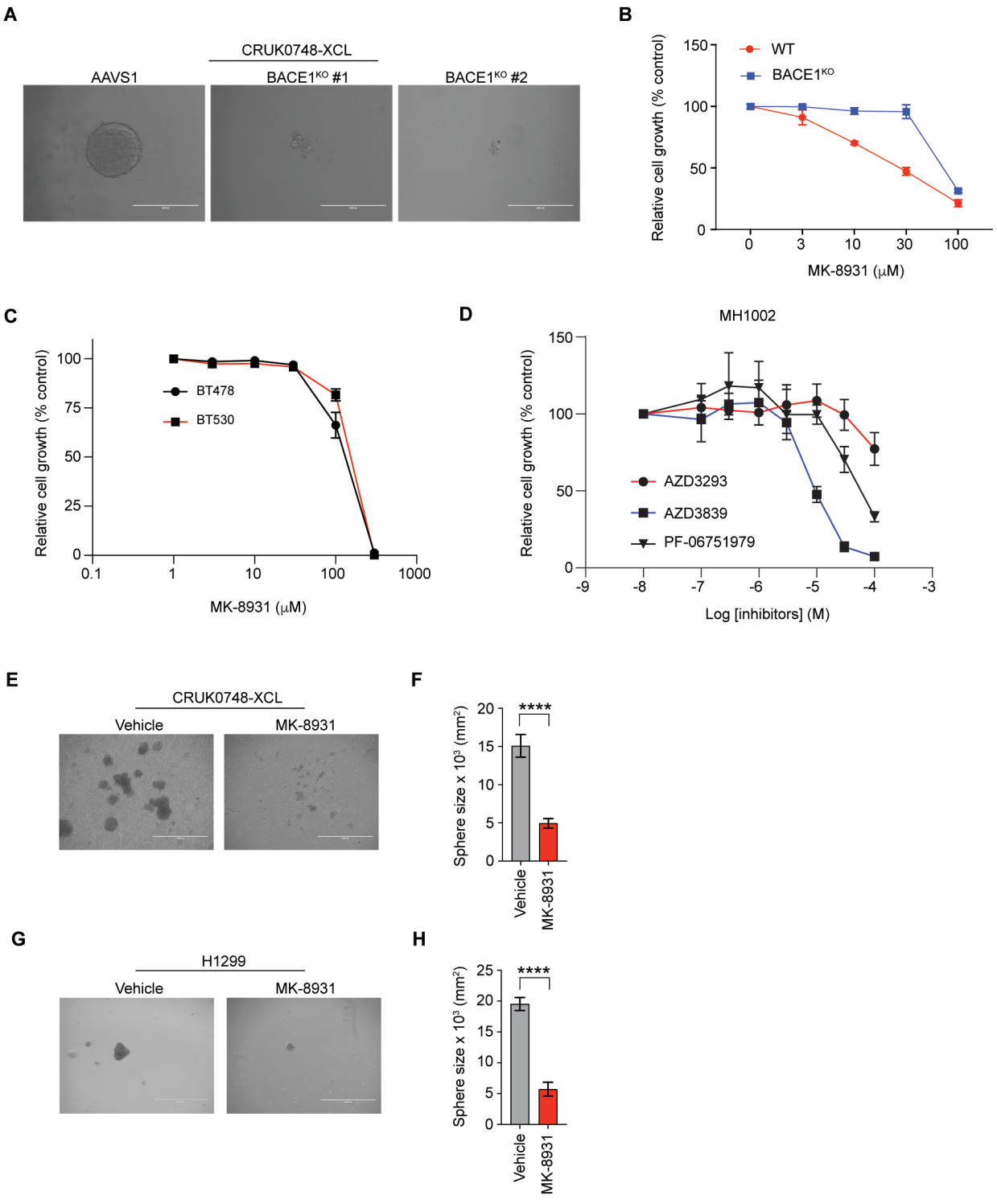
A
CRUK0748-XCL
AAVS1
BACE1KO #1
BACE1KO #2
B
WT
BACE1KO
Relative cell growth (% control)
MK-8931 (μM)
C
BT478
BT530
Relative cell growth (% control)
MK-8931 (μM)
D
MH1002
AZD3293
AZD3839
PF-06751979
Relative cell growth (% control)
Log [inhibitors] (M)
E
CRUK0748-XCL
Vehicle
MK-8931
F
Sphere size x 10³ (mm²)
****
Vehicle
MK-8931
G
H1299
Vehicle
MK-8931
H
Sphere size x 10³ (mm²)
****
Vehicle
MK-8931

Fig. S4. BACE1 is required for the proliferation and self-renewal capacity of LUAD brain metastases. (**A**) Micrographs of CRUK0748-XCL WT and BACE1^{KO} cells grown as spheres in stem cell enriching conditions for 7 days (*n*=6, *N*=2). Scale bar = 400 µm. (**B**) Growth of wild type and BACE1^{KO} MH1002 cells following treatment with the indicated concentrations of MK-8931 for 72 h (*n*=3, *N*=2). (**C**) Growth of lung-to-brain metastasis BMIC lines BT530 and BT478 following treatment with the indicated concentrations of MK-8931 for 72 hours (*n*=3, *N*=2). (**D**) Growth of MH1002 cells following treatment with the indicated BACE1 inhibitors for 72 hours (*n*=3, *N*=2). (**E**) Micrographs of CRUK0748-XCL cells in stem cell enriching conditions treated with 30 µM MK-8931 for 96 hours. Spheres were allowed to form for 7 days. Scale bar = 1000 µm. (**F**) Quantification of sphere size from cells imaged in (E) (*n*=6, *N*=3). (**G**) Micrographs of H1299 cells in stem cell enriching conditions treated with 30 µM MK-8931 for 96 hours. Spheres were allowed to form for 7 days. Scale bar = 1000 µm. (**H**) Quantification of sphere size from cells imaged in (G) (*n*=6, *N*=3). Data are presented as mean ± SEM. Data in (F) and (H) were analyzed by t test. **** *P*<0.0001.

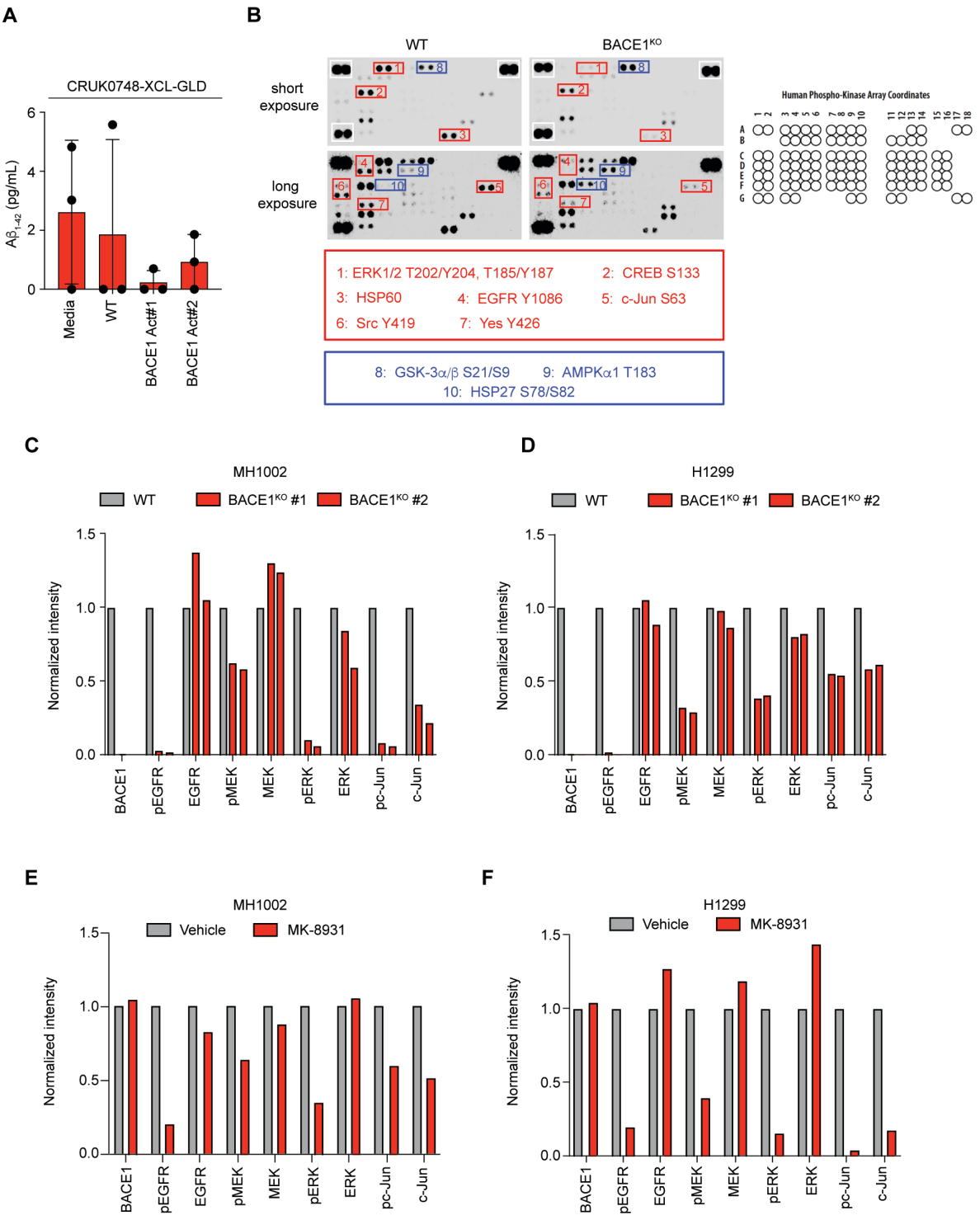

Fig. S5. BACE1 activates the EGFR/MEK/ERK axis in NSCLC. (**A**) $A\beta_{1\text{-}42}$ levels measured in the conditioned media from the indicated CRUK0748-XCL-GLD cell lines or media alone control (n=3, N=1). (**B**) (*Left*) Human Proteome Profiler™ phospho-kinase

antibody array in lysates from *BACE1*^{KO} MH1002 cells highlighting additional changes in kinase activity. Red – increased, Blue – decreased. (*Right*) Map of the Human Proteome Profiler™ phospho-kinase antibody array. (**C**) Quantification of signal intensity of the indicated proteins in lysates from MH1002 WT and BACE^{KO} cells. (**D**) Quantification of signal intensity of the indicated proteins in lysates from H1299 WT and BACE^{KO} cells. (**E**) Quantification of signal intensity of the indicated proteins in lysates from MH1002 cells treated with DMSO or 30 μm MK-8931 for 72 hours. (**F**) Quantification of signal intensity of the indicated proteins in lysates from MH1002 cells treated with DMSO or 30 μm MK-8931 for 72 hours.

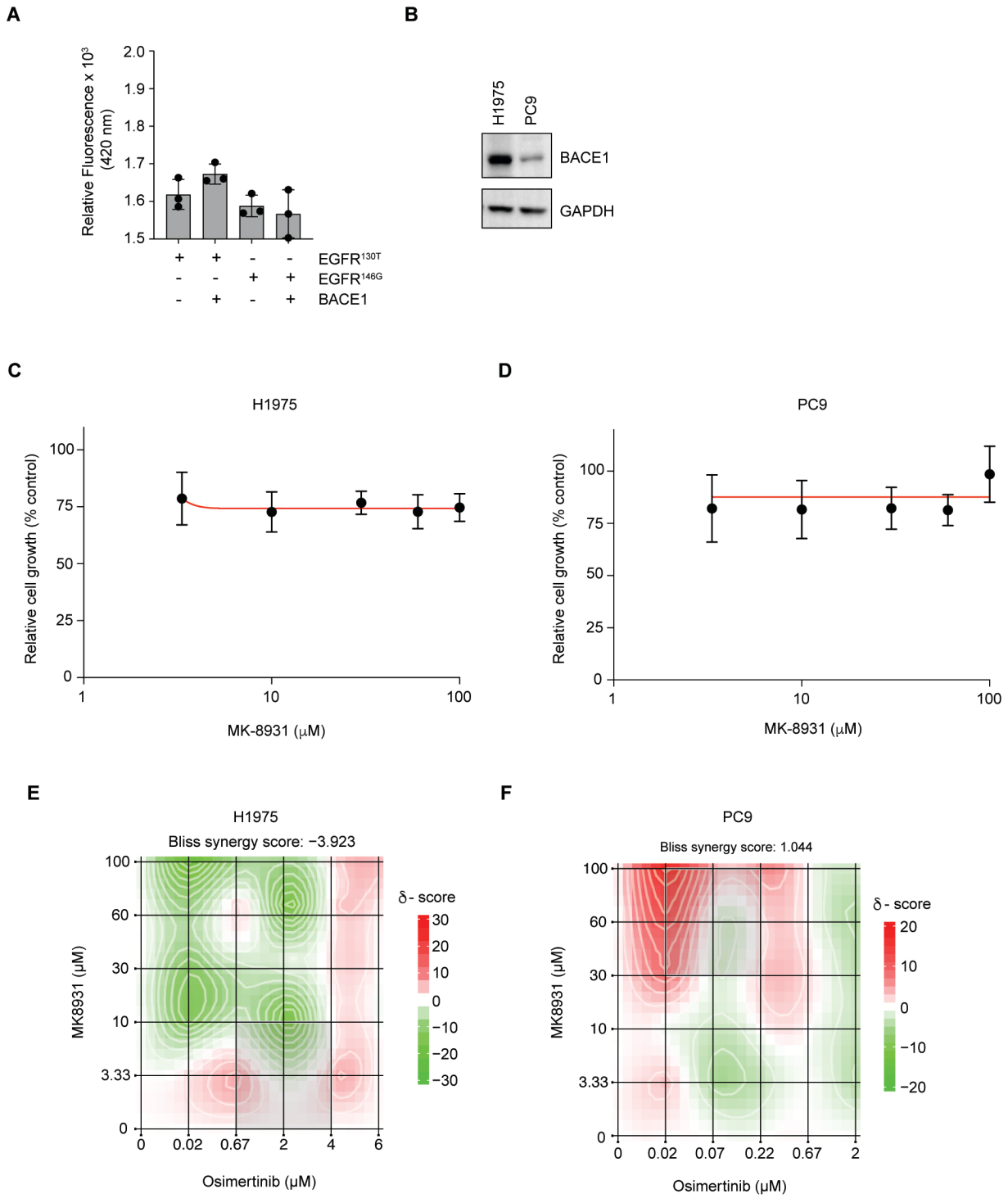
A
Relative Fluorescence x 10³ (420 nm)
2.0
1.9
1.8
1.7
1.6
1.5
+ + - - EGFR130T
- - + + EGFR146G
- + - + BACE1
B
H1975
PC9
BACE1
GAPDH
C
H1975
Relative cell growth (% control)
100
75
50
25
0
1
10
100
MK-8931 (μM)
D
PC9
Relative cell growth (% control)
100
75
50
25
0
1
10
100
MK-8931 (μM)
E
H1975
Bliss synergy score: −3.923
MK8931 (μM)
100
60
30
10
3.33
0
0 0.02 0.67 2 4 6
Osimertinib (μM)
δ - score
30
20
10
0
−10
−20
−30
F
PC9
Bliss synergy score: 1.044
MK8931 (μM)
100
60
30
10
3.33
0
0 0.02 0.07 0.22 0.67 2
Osimertinib (μM)
δ - score
20
10
0
−10
−20

Fig. S6. EGFR is a novel substrate of BACE1. (**A**) BACE1 (100 nM) was incubated with EGFR peptide (1 μM) encompassing the ^{130}T↓G^{131} or ^{146}G↓A^{147} cleavage site labelled with methyl coumarin and dinitrophenol FRET donor:acceptor pairs. The reactions were run for 24 hours at 37 °C. Bars indicate mean fluorescence at 420 nm ± standard deviation (*N*=2). (**B**) Western blot for BACE1 and GAPDH expression in the indicated EGFR mutant LUAD cell lines (*N*=2). Cell viability following treatment of EGFR mutant LUAD lines H1975 (**C**) and PC9 (**D**) for 72 hours with the indicated concentrations of MK-8931 (*n*=4, *N*=3). Topography plots displaying synergy scores of H1975 (**E**) and PC9 (**F**) determined using SynergyFinder 3.0 following treatment with the indicated concentrations of MK-8931 and Osimertinib (*45*). Synergy scores were determined using the BLISS model and BLISS scores are reported above each plot. Heatmaps indicate absolute synergy scores across the plots.

Table S1: Genetic information for patient-derived LUAD models

Cell line	Source	Sex	Age	TNM[a] Stage	Mutations	EGFR
CRUK0748	Here	Male	74	3a (T2b,N2,M0)	BRCA,KRAS G12V, KEAP1	WT
CRUK0733	Here	Male	66	3a (T2b,N2,M0)	TP53,ARID2,FBXW7	WT
MH1002	Here			M1b	KRAS G12D	WT
H1299	ATCC	Male	43		TP53	WT
H1975	ATCC	Female			PIK3CA, TP53	T790M; L858R
PC9	ATCC	Male	45		TP53	E746_A750del

[a] TNM staging AJCC version 8

Table S6: Primer sequences utilized for sgRNA amplification for NGS sequencing

Primer ID	Sequence
SCp7_01	CAAGCAGAAGACGGCATACGAGATCGGTTCAAGTGACTGGAGTTCAGACGTGTGCTC TT CCGATCTTCTACTATTCTTTCCCCTGCACTGT
SCp7_02	CAAGCAGAAGACGGCATACGAGATGCTGGATTGTGACTGGAGTTCAGACGTGTGCTC TT CCGATCTTCTACTATTCTTTCCCCTGCACTGT
SCp7_03	CAAGCAGAAGACGGCATACGAGATTAACTCGGGTGACTGGAGTTCAGACGTGTGCTC TT CCGATCTTCTACTATTCTTTCCCCTGCACTGT
SCp7_04	CAAGCAGAAGACGGCATACGAGATTAACAGTTGTGACTGGAGTTCAGACGTGTGCTCT T CCGATCTTCTACTATTCTTTCCCCTGCACTGT
SCp7_05	CAAGCAGAAGACGGCATACGAGATATACTCAAGTGACTGGAGTTCAGACGTGTGCTCT T CCGATCTTCTACTATTCTTTCCCCTGCACTGT
SCp7_06	CAAGCAGAAGACGGCATACGAGATGCTGAGAAGTGACTGGAGTTCAGACGTGTGCTC TT CCGATCTTCTACTATTCTTTCCCCTGCACTGT
SCp7_07	CAAGCAGAAGACGGCATACGAGATATTGGAGGGTGACTGGAGTTCAGACGTGTGCTC TT CCGATCTTCTACTATTCTTTCCCCTGCACTGT
SCp7_08	CAAGCAGAAGACGGCATACGAGATTAGTCTAAGTGACTGGAGTTCAGACGTGTGCTCT T CCGATCTTCTACTATTCTTTCCCCTGCACTGT
SCp7_09	CAAGCAGAAGACGGCATACGAGATCGGTGACCGTGACTGGAGTTCAGACGTGTGCTC TT CCGATCTTCTACTATTCTTTCCCCTGCACTGT
SCp7_10	CAAGCAGAAGACGGCATACGAGATTACAGAGGGTGACTGGAGTTCAGACGTGTGCTC TT CCGATCTTCTACTATTCTTTCCCCTGCACTGT
SCp7_11	CAAGCAGAAGACGGCATACGAGATATTGTCAAGTGACTGGAGTTCAGACGTGTGCTCT T CCGATCTTCTACTATTCTTTCCCCTGCACTGT
SCp7_12	CAAGCAGAAGACGGCATACGAGATTATGTCTTGTGACTGGAGTTCAGACGTGTGCTCT T CCGATCTTCTACTATTCTTTCCCCTGCACTGT
SCp7_13	CAAGCAGAAGACGGCATACGAGATATTGGATTGTGACTGGAGTTCAGACGTGTGCTCT T CCGATCTTCTACTATTCTTTCCCCTGCACTGT
SCp7_14	CAAGCAGAAGACGGCATACGAGATATACTCGGGTGACTGGAGTTCAGACGTGTGCTC TT CCGATCTTCTACTATTCTTTCCCCTGCACTGT
SCp7_15	CAAGCAGAAGACGGCATACGAGATTATGAGAAGTGACTGGAGTTCAGACGTGTGCTCT T CCGATCTTCTACTATTCTTTCCCCTGCACTGT
SCp7_16	CAAGCAGAAGACGGCATACGAGATGCACAGTTGTGACTGGAGTTCAGACGTGTGCTC TT CCGATCTTCTACTATTCTTTCCCCTGCACTGT
SCp7_17	CAAGCAGAAGACGGCATACGAGATCGTGGATTGTGACTGGAGTTCAGACGTGTGCTC TT CCGATCTTCTACTATTCTTTCCCCTGCACTGT
SCp7_18	CAAGCAGAAGACGGCATACGAGATTAGTAGAAGTGACTGGAGTTCAGACGTGTGCTCT T CCGATCTTCTACTATTCTTTCCCCTGCACTGT
SCp7_19	CAAGCAGAAGACGGCATACGAGATGCACGATTGTGACTGGAGTTCAGACGTGTGCTC TT CCGATCTTCTACTATTCTTTCCCCTGCACTGT
SCp7_20	CAAGCAGAAGACGGCATACGAGATCGGTAGCCGTGACTGGAGTTCAGACGTGTGCTC TT CCGATCTTCTACTATTCTTTCCCCTGCACTGT
SCp7_21	CAAGCAGAAGACGGCATACGAGATTAGTTCTTGTGACTGGAGTTCAGACGTGTGCTCT T CCGATCTTCTACTATTCTTTCCCCTGCACTGT
SCp7_22	CAAGCAGAAGACGGCATACGAGATTACAAGTTGTGACTGGAGTTCAGACGTGTGCTCT T CCGATCTTCTACTATTCTTTCCCCTGCACTGT
SCp7_23	CAAGCAGAAGACGGCATACGAGATATCACTGGGTGACTGGAGTTCAGACGTGTGCTC TT CCGATCTTCTACTATTCTTTCCCCTGCACTGT
SCp7_24	CAAGCAGAAGACGGCATACGAGATCGCATCAAGTGACTGGAGTTCAGACGTGTGCTC TT CCGATCTTCTACTATTCTTTCCCCTGCACTGT
SCp7_25	CAAGCAGAAGACGGCATACGAGATGCACGACCGTGACTGGAGTTCAGACGTGTGCTC TT CCGATCTTCTACTATTCTTTCCCCTGCACTGT
SCp7_26	CAAGCAGAAGACGGCATACGAGATTACACTCCGTGACTGGAGTTCAGACGTGTGCTC TT CCGATCTTCTACTATTCTTTCCCCTGCACTGT

SCp7_27	CAAGCAGAAGACGGCATACGAGATCGGTCTAAGTGACTGGAGTTCAGACGTGTGCTC TT CCGATCTTCTACTATTCTTTCCCCTGCACTGT
SCp7_28	CAAGCAGAAGACGGCATACGAGATATGTTCGGGTGACTGGAGTTCAGACGTGTGCTC TT CCGATCTTCTACTATTCTTTCCCCTGCACTGT
SCp7_29	CAAGCAGAAGACGGCATACGAGATCGTGGACCGTGACTGGAGTTCAGACGTGTGCTC TT CCGATCTTCTACTATTCTTTCCCCTGCACTGT
SCp7_30	CAAGCAGAAGACGGCATACGAGATATTGAGCCGTGACTGGAGTTCAGACGTGTGCTC TT CCGATCTTCTACTATTCTTTCCCCTGCACTGT
SCp5_01	AATGATACGGCGACCACCGAGATCTACACTCTTTCCCTACACGACGCTCTTCCGATCTT TGTGGAAAGGACGAAACACCG
SCp5_02	AATGATACGGCGACCACCGAGATCTACACTCTTTCCCTACACGACGCTCTTCCGATCT CTTGTGGAAAGGACGAAACACCG
SCp5_03	AATGATACGGCGACCACCGAGATCTACACTCTTTCCCTACACGACGCTCTTCCGATCT GCTTGTGGAAAGGACGAAACACCG
SCp5_04	AATGATACGGCGACCACCGAGATCTACACTCTTTCCCTACACGACGCTCTTCCGATCTA GCTTGTGGAAAGGACGAAACACCG
SCp5_05	AATGATACGGCGACCACCGAGATCTACACTCTTTCCCTACACGACGCTCTTCCGATCT CAACTTGTGGAAAGGACGAAACACCG
SCp5_06	AATGATACGGCGACCACCGAGATCTACACTCTTTCCCTACACGACGCTCTTCCGATCTT GCACCTTGTGGAAAGGACGAAACACCG
SCp5_07	AATGATACGGCGACCACCGAGATCTACACTCTTTCCCTACACGACGCTCTTCCGATCTA CGCAACTTGTGGAAAGGACGAAACACCG
SCp5_08	AATGATACGGCGACCACCGAGATCTACACTCTTTCCCTACACGACGCTCTTCCGATCT GAAGACCCTTGTGGAAAGGACGAAACACCG
pXPR502 _For	GAGGGCCTATTTCCCATGATTC
pXPR502 _Rev	CAAACCCAGGGCTGCCTTGGAA

Movie S1. Invasion of CRUK0733 cells.

Representative time lapse images from the Incucyte® of invading CRUK0733-XCL-GLD cells.

Movie S2. Invasion of CRUK0733 cells following increased expression of BACE1.

Representative time lapse images from the Incucyte® of CRISPR-activated *BACE1* (BACE1-act) CRUK0733-XCL-GLD cells.

.